

Nuclear structure of ^{231}Th from neutron capture and (d,p) reaction measurements

D. H. White,* H. G. Börner, and R. W. Hoff
Institut Laue-Langevin, 38042 Grenoble, France

and Lawrence Livermore National Laboratory, Livermore, California 94550

K. Schreckenbach, W. F. Davidson,† T. von Egidy,‡ D. D. Warner,§ P. Jeuch,** and G. Barreau††
Institut Laue-Langevin, 38042 Grenoble, France

W. R. Kane, M. L. Stelts,‡‡ R. E. Chrien, and R. F. Casten
Brookhaven National Laboratory, Upton, New York 11973

R. G. Lanier and R. W. Loughheed
Lawrence Livermore National Laboratory, Livermore, California 94550

R. T. Kouzes, R. A. Naumann, and R. Dewberry§§
Princeton University, Princeton, New Jersey 08540
 (Received 3 February 1986)

The nuclide ^{231}Th was investigated with the reactions $^{230}\text{Th}(n,\gamma)^{231}\text{Th}$, $^{230}\text{Th}(n,\gamma e)^{231}\text{Th}$, and $^{230}\text{Th}(d,p)^{231}\text{Th}$. Gamma rays from average resonance capture were measured, in addition to the usual thermal neutron capture spectroscopy. From these data, 70 excited levels in ^{231}Th were identified and, of these, 57 were placed in 18 rotational bands with assigned configurations. Candidates have been proposed for all expected Nilsson states below 750 keV, albeit with varying degrees of confidence, including the $\frac{5}{2}^+[622]$, $\frac{7}{2}^+[624]$, $\frac{3}{2}^- [761]$, $\frac{1}{2}^- [770]$, $\frac{1}{2}^+[640]$, and $\frac{5}{2}^- [503]$ configurations. Several vibrational states have been identified; a special feature of these is the observation of greater fragmentation of single-particle 0^+ phonon-mixed states than expected theoretically. Assuming degenerate parity doublets indicate the existence of stable octupole deformation, no evidence was found for a tendency toward this phenomenon in ^{231}Th . The neutron binding energy was determined to be 5118.13 ± 0.20 keV.

I. INTRODUCTION

Stable octupole deformation of light actinide nuclei has been recently discussed and evidence for its occurrence was found in ^{225}Ra .¹⁻³ Since it is expected that there exists a smooth transition from quadrupole to octupole deformation, the study of nuclei in this vicinity may shed new light on shape transitions in these heavy nuclei. An investigation of the level structure of an odd-mass nucleus in the actinide region below 1 MeV also provides information on excitations of single-particle states and the coupling of collective motion to these states.

The level structure of ^{231}Th has been studied previously by use of a variety of experimental techniques including spectroscopic determination of γ rays and/or particles emitted during α decay,⁴⁻⁸ β decay,⁸⁻¹¹ and single-nucleon-transfer reactions.¹²⁻¹⁶ The reactions used in previous investigations are all strongly selective and populate mainly levels with large components of single-particle excitation. By way of contrast, the (n, γ) reaction is less selective and is expected to populate all low-lying levels with spins within a range of a few units from that of the target spin. It has been shown already that the (n, γ) reaction is an excellent tool for use in identifying vibrations based on single particle states in odd-neutron nuclei.¹⁷ With the greatly increased resolving power and sensitivity of the new generation of β - and γ -ray spectrometers

operating at the High-Flux Reactor of the Institut Laue-Langevin (ILL) in Grenoble, extensive and detailed studies have already been made of other odd-neutron nuclei in the actinide region. Results have been published for level structure in the nuclei ^{227}Ra (Ref. 18), ^{233}Th (Ref. 19), ^{235}U (Ref. 20), ^{239}U (Ref. 21), and ^{249}Cm (Ref. 22). Thus, the use of neutron-capture gamma-ray spectroscopy held promise as a technique for producing an improved understanding of the ^{231}Th level structure.

II. EXPERIMENTAL METHODS

A. Secondary γ rays from thermal neutron capture

Secondary γ rays following thermal neutron capture in ^{230}Th ($\sigma_{\text{th}} = 23$ b) were measured using the curved-crystal spectrometers GAMS1 and GAMS2/3 at ILL. The target consisted of 49 mg of $^{230}\text{ThO}_2$ (enriched to 99.86%) in the form of a wafer of height 40 mm, depth 4 mm, and thickness 0.1 mm. The γ -ray spectrometers, which are installed at opposite ends of a transverse beam tube, view a common target situated in a thermal neutron flux of 5.5×10^{14} neutrons $\text{cm}^{-2} \text{s}^{-1}$. The GAMS1 spectrometer was used to study γ rays in the energy range 30–500 keV; the resolution obtained was full width at half maximum (FWHM)(keV) = $6.2 \times 10^{-6} E_{\gamma}^2(\text{keV})/n$, where n is the or-

der of diffraction, corresponding to a resolution of 20 eV at 100 keV in the third order of diffraction. The GAMS2/3 spectrometer was used to study γ rays in the energy range 150–1200 keV; the resolution obtained was $2.5 \times 10^{-6} E_\gamma^2 (\text{keV})/n$, corresponding to a resolution of 210 eV at 500 keV, also in the third order of diffraction. The two spectrometers, the standard measuring procedure, and the evaluation methods have been described in Ref. 23.

Several scans were taken with each instrument and data were collected for the first five orders of diffraction in the quartz crystals. The energies were calibrated relative to the Th $K\alpha_1$ x-ray energy; a value of 93.3483 keV was assumed from renormalizing Borchert's value²⁴ to the ^{198}Au absolute γ -ray standard of 411.8044 keV.²⁵ Intensity calibrations were obtained by folding the measured intensities with previously determined instrumental efficiency curves and correcting for self-absorption in the source. The experimental intensities were related to absolute intensities per 100 neutron captures by calibrating with several intense transitions in ^{231}Pa which arise from the beta decay of ^{231}Th (Ref. 26).

During the irradiation of the target in the high neutron flux, significant amounts of ^{231}Pa were produced (after ^{231}Th β decay). In addition to several ^{231}Th β -decay γ -ray lines that appeared in the spectrum, some ^{231}Pa capture gamma lines and ^{232}Pa β -decay lines²⁷ were observed. The former were assigned by comparison with a separate (n, γ) measurement on a ^{231}Pa target. Gamma rays from these various extraneous sources, β decay, fission products,²⁸ and second-order neutron capture, were removed from the compilation. Since the destruction of the ^{230}Th target material was slow during the 10–20 d irradiations, γ rays whose intensities changed significantly with time were attributed to buildup products and, identified or not, were

eliminated. The complete set of 278 γ -ray energies and intensities attributed to ^{231}Th is given in Table I.

B. Conversion electrons from thermal neutron capture

The conversion electrons following thermal neutron capture in ^{230}Th have been studied with the BILL β spectrometer at ILL.²⁹ The target consisted of 6 mg $^{230}\text{ThO}_2$ enriched to 99.86% in ^{230}Th . It was produced by electro-deposition onto a nickel substrate ($2300 \mu\text{g}/\text{cm}^2$) forming a thin layer measuring $30 \times 100 \text{ mm}$; the Th surface density was $200 \mu\text{g}/\text{cm}^2$. The thermal neutron flux at the in-pile target position was 3×10^{14} neutrons $\text{cm}^{-2} \text{ s}^{-1}$.

Conversion electrons were recorded in the range $70 < E_e < 900 \text{ keV}$ using a five-wire proportional counter. The momentum resolution obtained was $\Delta p/p = 5 \times 10^{-4}$. Multipolarities of strong transitions were determined by the L -subshell ratios and pure multipolarities were selected for the relative intensity calibration between the (n, γ) and the (n,e) measurements. Multipolarities of weaker transitions could then be deduced from the absolute coefficients.³⁰ In several cases the absence of a conversion electron line set an upper limit on the conversion coefficient, resulting in some information on the multipolarity (e.g., identifying the transition as $E1$ or $E2$). In a few instances, transitions have been identified from their conversion electron lines even though no photon has been detected. These are listed in Table II, with the experimental conversion coefficient indicated as a lower limit. The measured conversion electron energies, conversion coefficients, and deduced multipolarities are listed together with the γ -ray energies in Table II. Spectra for conversion electrons with energies in the range 320–440 keV are shown in Fig. 1. This region is of particular importance because several transitions are found to exhibit unusually

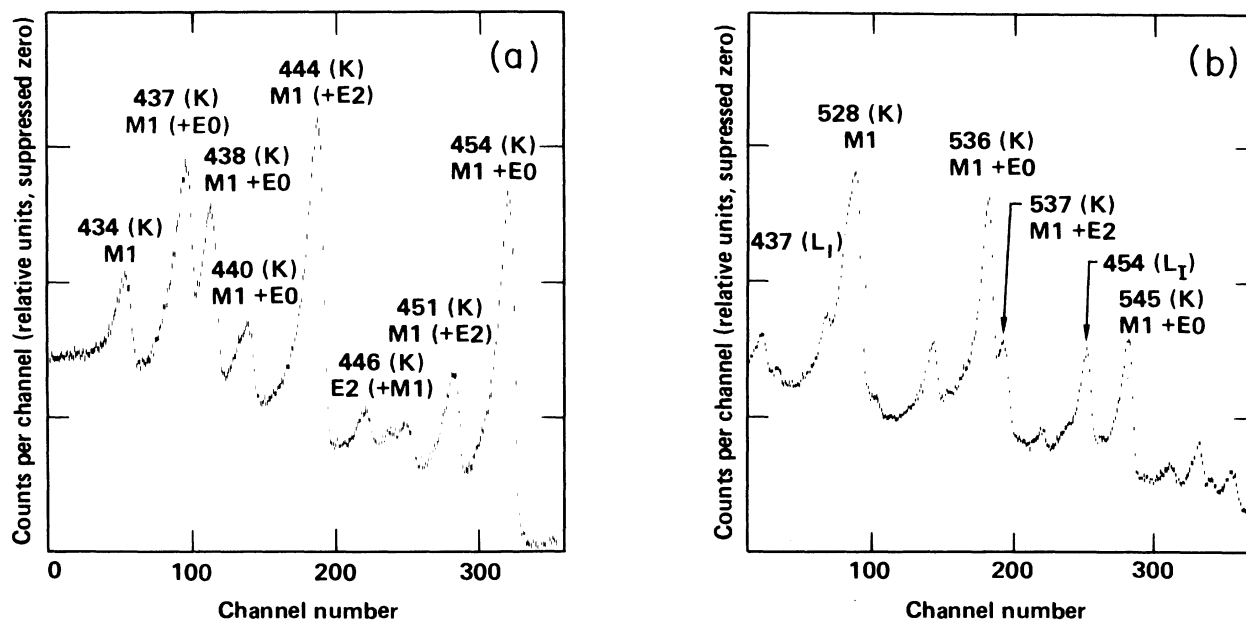


FIG. 1. (a) and (b) Conversion electron spectra taken with the BILL spectrometer in an energy range where conversion coefficients indicate appreciable $E0$ mixing in transitions.

TABLE I. Gamma-ray transition energies and intensities (errors of the last digits in parentheses) from the $^{230}\text{Th}(n,\gamma)^{231}\text{Th}$ reaction and measured with the GAMS1 and GAMS2/3 spectrometers. (Multipol. denotes multipolarity.)

Gamma energy ^a (keV)	Intensity (per 100 n) ^b	Multipol. ^c	Gamma energy ^a (keV)	Intensity (per 100 n) ^b	Multipol. ^c	Gamma energy ^a (keV)	Intensity (per 100 n) ^b	Multipol. ^c
47.356(6)	0.15(4)		248.586(9)	0.047(9)	M1	385.532(3)	0.25(4)	A E1,E2*
47.807(7)	0.17(5)		255.365(11)	0.031(6)	A M1	388.482(9)	0.083(13)	A
53.674(7)	0.15(4)		255.903(10)	0.031(6)	A	390.662(4)	0.17(3)	A M1+E2
55.417(6)	0.14(4)		259.790(4)	0.140(21)	A M1+E2	391.619(13)	0.048(10)	M1
57.984(4)	0.26(7)		272.181(2)	0.62(9)	A M1+E2	392.038(13)	0.048(10)	A
59.323(4)	0.39(10)		275.129(2)	0.65(10)	A M1+E2	398.242(10)	0.073(15)	A E1,E2*
66.26(3)	0.063(21)		275.428(4)	0.17(3)	A M1(+E2)	405.121(3)	1.00(15)	A E2+M1
67.263(6)	0.082(13)		278.524(14)	0.028(6)	A	407.899(2)	1.56(24)	A E2
76.198(4)	0.128(19)	A	281.441(9)	0.088(14)	A M1	410.252(10)	0.079(16)	A M1
80.347(2)	0.20(3)	A	282.471(2)	2.2(3)	A E1	415.460(8)	0.081(13)	A M1
89.443(1)	1.29(24)		284.659(13)	0.028(6)	A	417.201(7)	0.112(18)	E2
95.713(8)	0.21(3)		289.092(10)	0.030(6)	A	417.793(14)	0.054(12)	A M1
106.183(7)	0.25(4)		295.037(15)	0.031(6)	A	418.62(4)	0.012(2)	A
107.591(4)	0.116(21)		301.741(3)	0.39(6)	A M1	419.031(16)	0.052(11)	A M1
112.393(12)	0.080(12)		302.540(7)	0.053(11)	A E1,E2*	424.032(4)	0.36(6)	A M1+E2
143.764(2)	3.2(5)	A E1	307.063(2)	1.63(25)	A E1	424.43(3)	0.043(9)	M1
145.961(25)	0.066(13)		309.557(12)	0.039(8)	A E1,E2*	427.110(7)	0.105(16)	A M1
147.599(3)	0.032(6)		311.897(7)	0.052(11)	A	428.71(4)	0.023(5)	A M1+E0
148.693(12)	0.083(13)	M1	317.062(12)	0.030(6)	A M1	433.517(8)	0.135(22)	A E2 or E1
160.604(13)	0.028(5)		317.886(22)	0.015(3)	A	433.927(4)	0.19(3)	A M1
163.358(2)	0.41(6)	A E1,E2*	318.672(4)	0.110(17)	E2+M1	436.917(4)	0.28(4)	A M1(+E0)
179.297(2)	0.27(4)	A M1(+E2)	320.899(4)	0.105(16)	A M1(+E2)	438.22(2)	<0.025	A M1+E0
182.500(8)	0.078(16)	A	321.435(4)	0.099(15)	E1,E2*	439.427(11)	0.073(15)	A M1+E2
185.712(1)	18.0(27)	A E1	323.794(2)	0.27(4)	A E1,E2*	440.044(7)	0.121(19)	A M1+E0
198.928(2)	1.8(3)	A M1	325.925(3)	0.17(3)	A	441.64(4)	0.035(7)	A
200.292(19)	0.046(9)		332.479(7)	0.047(9)	E1,E2*	443.626(2)	0.94(14)	A M1(+E2)
202.111(3)	0.21(3)	A M1	336.240(10)	0.041(8)	A M1	444.892(14)	0.076(16)	A E1,E2*
203.566(9)	0.066(13)		337.569(9)	0.042(9)	M1	448.339(18)	0.02(1)	A
205.309(2)	0.35(5)	A E1,E2*	342.702(17)	0.025(5)	A M1	445.996(7)	0.137(21)	A E2(+M1)
211.608(3)	0.136(21)	M1	343.247(3)	0.25(4)	E2+M1	450.680(4)	0.30(5)	M1(+E2)
215.638(6)	0.085(13)	M1	346.015(4)	0.21(3)	E1,E2*	453.50(6)	0.07(2)	M1+E0
221.399(1)	9.6(15)	A M1	351.512(23)	0.025(5)	A M1	454.19(7)	0.046(11)	M1+E2
228.785(6)	0.086(13)	A M1	354.721(20)	0.025(5)	A	456.990(11)	0.110(19)	A E2(+M1)
230.243(11)	0.034(7)		360.982(22)	0.037(7)	M1	459.22(8)	0.046(13)	A
233.469(3)	0.68(10)	A M1	368.934(2)	0.77(12)	A E2	460.753(3)	0.54(8)	M1
239.548(4)	0.40(6)	A M1	372.221(2)	0.64(10)	A E1	461.571(7)	0.17(3)	M1
240.875(3)	2.6(4)	A M1(+E2)	372.855(11)	0.080(13)	E1,E2*	463.085(12)	0.101(22)	A E2+M1
244.451(10)	0.048(10)	A E1	374.590(9)	0.063(13)	A E1,E2*	466.227(3)	0.54(8)	A M1
247.586(3)	0.140(21)	A E2	381.934(24)	0.045(10)	M1	467.172(20)	0.072(18)	M1+E2
						468.209(19)	0.074(16)	A M1(+E2)

TABLE I. (Continued).

Gamma energy ^a (keV)	Intensity (per 100 n) ^b	Multipol. ^c	Gamma energy ^a (keV)	Intensity (per 100 n) ^b	Multipol. ^c	Gamma energy ^a (keV)	Intensity (per 100 n) ^b	Multipol. ^c
468.944(10)	0.132(21)	M1(+E2)	567.108(19)	0.096(16)	A M1+E0	696.01(4)	0.066(15)	
470.25(3)	0.037(9)	A M1	567.570(16)	0.17(3)	M1	696.85(6)	0.043(10)	
475.62(7)	0.11(3)	E2+M1	570.4(1)	0.03(2)	M1	705.53(17)	0.032(10)	
479.19(5)	0.12(2)	A E2	572.964(7)	0.24(4)	A M1+E0	707.1(3)	0.054(13)	
479.45(7)	0.10(3)		585.607(13)	0.111(18)	A	709.220(14)	0.56(9)	A E2+M1
482.62(5)	0.026(6)	A	587.155(17)	0.081(14)	A M1	713.234(16)	0.20(3)	A M1(+E2)
483.507(17)	0.060(13)	A M1+E2	593.86(3)	0.054(12)	M1	717.99(4)	0.084(15)	M1
485.256(4)	0.25(4)	M1	596.40(11)	0.011(10)		719.74(12)	0.037(9)	A
486.79(3)	0.053(12)		599.20(4)	0.050(11)	A	726.19(3)	0.091(16)	
487.689(23)	0.057(12)	A E1,E2*	604.467(24)	0.073(16)		729.19(5)	0.082(13)	A M1(+E2)
488.55(5)	0.023(5)	A	611.80(2)	0.093(15)	A	736.73(17)	0.032(8)	
489.43(4)	0.053(11)	M1+E2	612.50(10)	0.043(11)		739.409(25)	0.139(23)	A M1+E0
490.51(2)	0.057(12)	A M1	613.84(7)	0.033(8)	M1	749.14(5)	0.095(15)	A M1
491.284(4)	0.34(5)	A E2	614.563(14)	0.132(21)	A M1	750.621(16)	0.23(4)	A M1
493.177(25)	0.050(10)	A E1,E2*	617.87(4)	0.047(10)	A M1(+E0)	755.23(10)	0.075(16)	M1
498.775(2)	1.25(19)	A M1	619.27(13)	0.068(2)	A	757.28(18)	0.048(11)	A
503.44(6)	0.045(11)	A	619.67(4)	0.046(10)	M1	758.38(4)	0.097(16)	M1
506.74(7)	0.045(10)	A	621.45(5)	0.037(8)		763.363(24)	0.16(3)	A M1
514.32(3)	0.096(16)	M1+E0	626.64(4)	0.055(12)	A	766.6(3)	0.043(11)	A
514.991(7)	0.47(7)	A M1+E2	628.394(25)	0.084(14)	M1	768.43(18)	0.047(11)	
520.847(14)	0.102(16)	A E2+M1	629.368(15)	0.090(14)	A	771.60(9)	0.069(15)	
522.218(16)	0.089(14)	A M1	630.00(6)	0.061(13)	A E2	773.18(13)	0.047(11)	A
523.90(5)	0.037(9)		632.41(7)	0.022(4)	M1	775.04(13)	0.052(15)	A
526.68(5)	0.033(8)	A M1	643.85(7)	0.037(9)	A	783.56(8)	0.098(16)	
528.038(3)	0.70(11)	A M1	646.422(17)	0.16(3)		784.05(9)	0.106(20)	A
533.82(3)	0.031(7)	M1	647.528(5)	0.64(10)	M1	785.08(8)	0.104(17)	A
534.562(15)	0.072(15)	A M1	649.142(23)	0.102(16)	A M1	787.13(7)	0.077(17)	
535.36(8)	0.05(1)	M1	655.25(4)	0.052(12)	E2(+M1)	793.04(3)	0.115(23)	A
536.336(17)	0.076(16)	A M1+E0	658.97(6)	0.040(9)	A E2+M1	797.56(13)	0.063(14)	A
537.307(8)	0.28(4)	M1+E2	662.55(7)	0.043(11)		799.38(5)	0.093(16)	A
539.27(5)	0.028(7)		664.95(12)	0.032(8)	E2+M1	803.49(6)	0.103(17)	
541.11(8)	0.022(4)		667.185(12)	0.27(4)	E2	807.65(4)	0.18(3)	
543.66(3)	0.033(7)	A M1	668.56(10)	0.054(12)	A E2+M1	808.38(9)	0.10(3)	A
545.420(16)	<0.025	A M1+E0	672.75(12)	0.028(8)	M1	808.74(9)	0.093(16)	A
548.454(15)	0.083(13)	A E2+M1	673.96(13)	0.05(2)	A	811.408(15)	0.38(6)	A E2
549.02(5)	0.041(9)		678.1(3)	0.032(10)	A	814.64(4)	0.148(24)	A E1,E2*
552.34(4)	0.024(5)	M1+E0	681.37(7)	0.096(16)	A E2+M1	816.70(9)	0.070(15)	A
554.23(5)	0.022(4)		684.131(13)	0.23(4)	E2(+M1)	820.43(7)	0.089(15)	A
555.53(5)	0.013(3)		687.658(7)	0.67(10)	A E2	827.05(4)	0.141(22)	M1
556.76(7)	0.063(13)	M1+E2	688.611(24)	0.17(3)	A E2+M1	834.92(5)	0.138(22)	A M1
560.875(21)	0.058(12)	A	689.932(8)	0.49(8)	M1	836.56(8)	0.096(16)	

TABLE I. (Continued).

Gamma energy ^a (keV)	Intensity (per 100 n) ^b	Multipol. ^c	Gamma energy ^a (keV)	Intensity (per 100 n) ^b	Multipol. ^c	Gamma energy ^a (keV)	Intensity (per 100 n) ^b	Multipol. ^c
839.36(5)	0.139(22)	A	921.19(24)	0.091(17)		1024.91(25)	0.069(23)	A
841.24(16)	0.041(10)	E1, E2*	930.55(14)	0.101(18)	M1	1029.17(18)	0.092(19)	
844.55(18)	0.042(10)	A	936.17(6)	0.23(4)	A	1035.23(8)	0.16(3)	
855.01(13)	0.079(17)	M1+E0	938.72(10)	0.16(3)		1039.91(20)	0.073(21)	A
861.86(24)	0.042(10)	A	950.11(15)	0.110(22)		1066.07(15)	0.077(25)	
870.00(11)	0.089(14)		952.79(6)	0.26(4)	M1	1084.86(14)	0.14(3)	
875.54(7)	0.126(21)	A	971.86(20)	0.14(4)		1091.26(10)	0.20(4)	
866.15(25)	0.059(14)	A	974.15(16)	0.059(18)	A	1116.44(10)	0.17(4)	
888.49(19)	0.068(15)	A	982.44(7)	0.44(8)		1144.43(20)	0.098(23)	
905.12(9)	0.124(21)		983.46(6)	0.35(7)		1186.82(12)	0.38(7)	
911.87(11)	0.063(15)	M1	1012.83(13)	0.29(6)		1220.5(4)	0.14(3)	
914.91(7)	0.148(24)	A	1014.33(4)	0.41(8)	A			E2, E1
918.92(11)	0.098(16)	A	1019.96(22)	0.108(20)				

^aErrors of the last digits are in parentheses. The gamma energies were obtained from conversion electron measurements if the intensity is given as an upper limit.

^bErrors of the last digits are in parentheses. The listed error consists of a 15% systematic calibration error added in quadrature to the statistical error.

^cA means the transition has been assigned a place in the level scheme. An asterisk means the possible multipolarities were deduced from an estimated upper limit for the conversion electron intensity.

TABLE II. Conversion coefficients for transitions from the $^{230}\text{Th}(n, \gamma e)^{231}\text{Th}$ reaction, where electrons were measured with the BILL spectrometer.

Gamma energy (keV)	Shell	Expt. conv. coeff.	Gamma energy (keV)	Shell	Expt. conv. coeff.	Gamma energy (keV)	Shell	Expt. conv. coeff.
148.693	L1	1.8(3)	215.638	K	1.64(25)	248.586	K	1.4(3)
179.297	L1	0.48(7)	228.785	K	1.45(22)	255.365	K	1.21(25)
	L2	0.17(3)	233.469	K	1.32(20)		L1	0.24(5)
	M1	0.127(19)		L1	0.18(3)	259.790	K	0.71(11)
185.712	K	0.066(10)		M1	0.051(8)		L1	0.19(3)
	L1	0.011(2)		N1	0.031(5)	272.181	K	0.60(9)
	L2	0.005(1)	239.548	K	1.53(23)		L1	0.120(18)
	L3	0.002(1)		L1	0.28(4)		L2	0.013(2)
	M1	0.001(1)		M1	0.101(15)		M1	0.038(6)
198.928	K	2.7(4)		N1	0.057(9)	275.132	K	0.60(9)
	L1	0.36(5)		K	1.24(19)		L1	0.159(24)
	L2	0.036(5)		L1	0.21(3)		M1	0.028(4)
202.111	K	0.083(13)		L2	0.041(6)		K	0.73(11)
	M1	2.2(3)		M1	0.058(9)		L1	1.23(19)
	L1	0.33(5)		N1	0.011(2)		K	0.74(12)
211.608	K	1.8(3)	247.586	L2	0.30(5)		K	0.034(5)
	L1	0.39(6)		L3	0.071(11)		L1	0.011(2)

TABLE II. (Continued).

Gamma energy (keV)	Shell	Expt. conv. coeff.	Multipol.	Gamma energy (keV)	Shell	Expt. conv. coeff.	Multipol.	Gamma energy (keV)	Shell	Expt. conv. coeff.	Multipol.
567.570	L2	0.033(10)		649.142	L1	0.013(2)		749.14	K	0.082(7)	M1
	K	0.091(14)	M1	655.25	K	0.068(6)		750.621	K	0.063(5)	M1
570.40	L1	0.019(4)		658.97	K	0.036(7)	M1	755.23	K	0.094(21)	M1
	K	0.22(9)	M1	664.95	K	0.050(9)	E2(+M1)	758.38	K	0.060(10)	M1
572.964	K	0.45(7)	M1+E0	667.185	K	0.043(12)	E2(+M1)	763.363	K	0.056(8)	M1
	K	0.080(8)		668.56	K	0.013(1)	E2	811.408	K	0.014(2)	E2
587.155	L1	0.110(11)	M1	672.75	K	0.043(12)	E2+M1	827.05	K	0.043(7)	M1
	K	0.039(5)		681.37	K	0.081(24)	M1	834.92	K	0.042(7)	M1
593.86	K	0.15(3)	M1	684.131	K	0.04(4)	E2+M1	855.01	K	0.14(3)	M1
613.84	K	0.103(15)	M1	687.658	K	0.037(2)	E2(+M1)	911.87	K	0.054(13)	M1
614.563	K	0.105(6)	M1	688.611	K	0.019(1)	E2	927.9	K	0.030(7)	M1
617.87	K	0.220(20)	M1(+E0)	689.932	K	0.040(5)	E2+M1	930.55	K	0.032(6)	M1
619.67	K	0.150(20)	M1	709.220	L1	0.086(4)	M1	945.75	K	0.014(3)	E2(+M1)
628.394	K	0.082(8)	M1	713.234	K	0.010(2)		952.79	K	0.042(7)	M1
630.00	K	0.016(3)	E2	739.409	K	0.046(3)	E2+M1	1014.33	K	0.005(1)	E2,E1
632.41	K	0.10(8)	M1		K	0.052(4)	M1(+E2)				
647.528	K	0.078(12)	M1		K	0.132(10)	M1+E0				

large conversion coefficients due to the presence of $E0$ admixtures in their multiplicities.

C. Primary γ rays from thermal neutron capture

Primary γ rays following thermal capture were measured with a three-crystal pair spectrometer located downstream of the GAMS1 spectrometer at ILL. The pair spectrometer³¹ consists of a Ge(Li) detector, flanked by two NaI(Tl) counters for coincident detection of 511 keV annihilation quanta. The data were taken in several separate runs. These spectra were combined and the resulting spectrum was analyzed for peaks in the interval 3800–5200 keV. Aluminum and carbon, materials of construction in the source assembly, produced strong primary capture peaks. The energies of these impurities, which have been determined accurately in previous work,³² were used to calibrate the spectrum. The γ rays attributed to primary transitions following thermal neutron capture in ^{230}Th are listed in Table III.

D. Primary γ rays from average resonance neutron capture

Primary γ rays following average resonance neutron capture (ARC) have been measured using a three-crystal pair spectrometer^{32,33} at the Brookhaven High-Flux Beam Reactor. The target consisted of 10 g of ThO_2 enriched to 83.86% in ^{230}Th . Measurements were made with a neutron beam of average energy 2 keV that was produced by transmission through a scandium filter. Typical energy resolution was $\text{FWHM}=5.5$ keV at 4.5 MeV. The energies and relative intensities of the observed transitions are listed in Table III. The reduced intensities are plotted as a function of excitation energy and are compared in Fig. 2

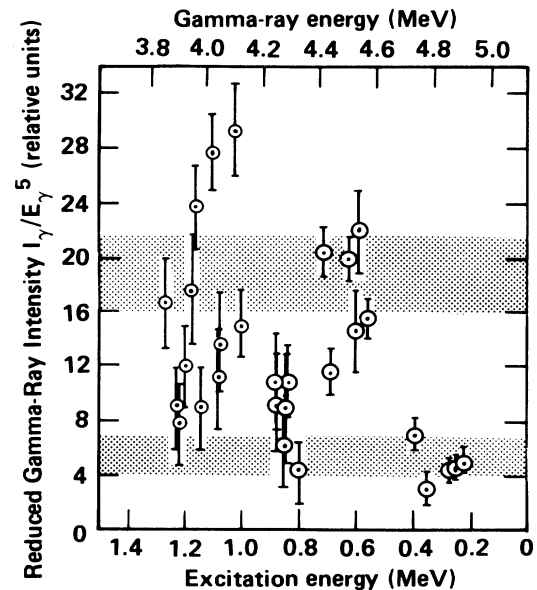


FIG. 2. Reduced gamma-ray intensities from 2-keV average resonance capture (ARC) measurements. The shaded areas indicate calculated intensities for gammas feeding levels with $I^\pi = \frac{1}{2}^-, \frac{3}{2}^-$ (upper) and $I^\pi = \frac{1}{2}^+, \frac{3}{2}^+$ (lower).

with calculated intensities based on a Monte Carlo simulation of the averaging process.³⁴ It is assumed that the peaks represented by the two points of highest gamma intensity in Fig. 2 are both multiplets. Since the target size was rather small for this technique, the measurement was marginal in terms of being certain that transitions popu-

lating all $I = \frac{1}{2}$ and $\frac{3}{2}$ states were observed. Inspection of the spectrum suggests that one may assume all negative parity states with $I = \frac{1}{2}$ and $\frac{3}{2}$ have been identified up to 1200 keV excitation. As will be shown in Sec. III, there are four peaks below 1.2-MeV excitation energy in the ARC spectrum [corresponding to level energies of

TABLE III. Primary gamma rays from thermal and 2-keV resonance capture in ²³⁰Th. (Multipol. denotes multipolarity.)

Thermal neutron capture			Average resonance capture		
E_γ ^a (keV)	E_{level} (keV)	I_γ (rel)	E_{level} (keV)	I_γ (rel)	Multipol.
5117.69(17)	0.36(17)	0.59(4)			
4896.82(21)	221.24(21)	0.95(8)	221.4(7)	15(3)	M1
4870.1(3)	248.0(3)	0.34(4)	247.2(7)	13(3)	M1
4845.92(6)	272.14(7)	2.16(11)	272.0(7)	12(3)	M1
4769.8(5)	348.2(5)	0.50(8)	349.7(10)	8(3)	M1
4738.1(3)	380.0(3)	1.8(3)			
			386.5(5)	17(3)	M1
4616.9(5)	501.1(5)	0.35(5)			
4581.4(7)	536.7(7)	0.20(4)			
4563.45(9)	554.62(10)	6.5(3)	555.0(3)	31(3)	E1
4527.09(11)	590.98(11)	8.2(5)	591.4(7)	42(12)	E1
4523.95(25)	594.12(25)	2.0(3)	595.2(9)	28(12)	E1
4498.5(3)	619.5(3)	0.30(5)	619.9(3)	37(3)	E1
4462.2(3)	655.9(3)	0.32(4)			
			685.6(5)	20(3)	E1, M1
4424.61(17)	693.46(17)	1.74(12)			
4404.39(11)	713.68(11)	5.1(3)	713.2(3)	34(3)	E1
			794.2(12)	7(3)	M1
4297.14(21)	820.94(21)	1.10(10)			
4284.91(12)	833.17(12)	13.1(7)	834.5(8)	16(4)	E1, M1
4278.73(17)	839.35(17)	2.71(18)	840.1(14)	13(6)	E1, M1
			843.7(16)	9(4)	M1
4271.7(4)	846.3(4)	0.50(7)			
			869.9(11)	13(5)	E1, M1
4242.45(15)	875.63(15)	2.29(15)	874.9(10)	15(5)	E1, M1
4218.9(6)	899.2(6)	0.18(4)			
4182.51(19)	935.57(19)	0.91(7)	no peak		
4175.9(9)	942.2(9)	0.17(5)			
4157.42(17)	960.66(17)	1.13(8)	weak peak		
4113.98(13)	1004.11(13)	3.37(19)	1003.8(5)	18(3)	E1, M1
4096.72(13)	1021.37(13)	3.47(19)	1021.0(3)	34(4)	E1
4085.1(3)	1033.0(3)	0.47(6)			
4062.44(13)	1055.65(13)	2.45(14)			
			1075.1(8)	15(4)	E1, M1
			1081.2(9)	12(4)	E1, M1
4023.87(23)	1094.22(23)	0.69(7)			
			1103.3(4)	29(3)	E1
3981.82(17)	1136.27(17)	1.23(9)	1134.3(26)	9(3)	(M1)
3962.6(4)	1155.5(4)	0.93(15)			
3958.49(12)	1159.64(12)	9.8(5)	1159.1(4)	23(3)	E1
3946.19(24)	1171.90(24)	0.73(7)	1172.7(6)	17(4)	E1, M1
3924.9(8)	1193.2(8)	0.19(6)			
3917.71(17)	1200.38(17)	1.47(10)	1202.0(8)	11(3)	E1, M1
3904.26(21)	1213.83(21)	1.28(10)			
3899.07(24)	1219.02(24)	1.06(10)	1219.1(32)	7(3)	(M1)
			1222.0(29)	8(3)	(M1)
3866.66(17)	1251.43(17)	1.23(9)			
3843.6(4)	1274.5(4)	0.51(8)	1271.3(6)	14(3)	E1

^aEnergy not corrected for recoil.

349.7(10), 386.5(5), 843.7(16), and 869.9(11) keV], where no conclusive evidence was found for the existence of a level from either thermal-capture or (d,p) spectroscopy. Although the ARC spectrum was checked rigorously for the presence of contaminant lines, these peaks may possibly be spurious since one would expect to find corroborating evidence for levels with $I < \frac{7}{2}$ from the other experimental probes, especially at the lower excitation energies.

E. Proton spectra from the (d,p) reaction

The proton spectra from the $^{230}\text{Th}(d,p)^{231}\text{Th}$ reaction were measured by use of a quadrupole three-dipole (Q3D) spectrometer³⁵ at the Princeton cyclotron facility. The target consisted of $100 \mu\text{g}/\text{cm}^2$ ^{230}Th (isotopic purity $> 99.9\%$) deposited on a $40 \mu\text{g}/\text{cm}^2$ carbon backing. The detector in the Q3D spectrometer consisted of a 60-cm resistive-division position-sensitive gas proportional counter filled with 0.3 atm pure propane backed by a plastic scintillator. The position accuracy of the proportional counter was better than 1 mm. Particle identification was obtained by examining the total proportional counter signal versus the scintillator signal.

The energy of the incident deuteron beam was 20 MeV. Spectra were collected at 5° intervals from 15° to 75° , typically requiring 2 h per run. An overall resolution of 10 keV was obtained. A typical spectrum is shown in Fig. 3. The excitation energies corresponding to observed peaks and measured cross sections are listed in Table IV. Relative cross-section values were obtained by normalization to the elastically scattered deuteron peak which was recorded during short exposures taken before and after each run. Due to some problems with the solid-state detector used for this purpose, the data at higher angles (60° – 75°) had to be renormalized; the intense peak at 326 keV, which involves an $l=4$ angular momentum transfer, was used for this renormalization. The experimental cross sections were put on an absolute scale by normalizing to calculated values for the 248- and 271-keV peaks ($\theta=40^\circ$), which are the first two members of the $\frac{1}{2}^+$ [631] band in ^{231}Th . This absolute scale, which appears in Table IV and Figs. 3 and 4, is uncertain by about $\pm 25\%$.

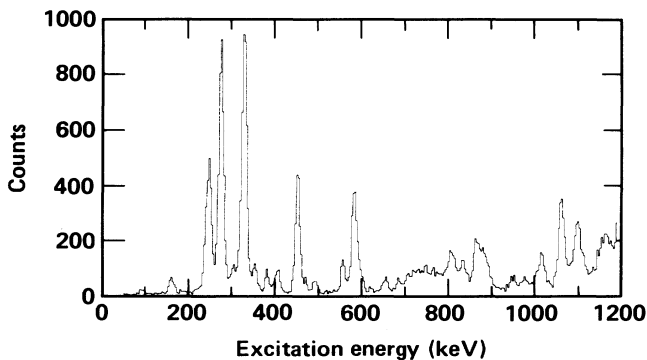


FIG. 3. The proton spectrum obtained with a Q3D spectrometer from a measurement of the reaction $^{230}\text{Th}(d,p)^{231}\text{Th}$; $E_d=20$ MeV and $\theta=40^\circ$.

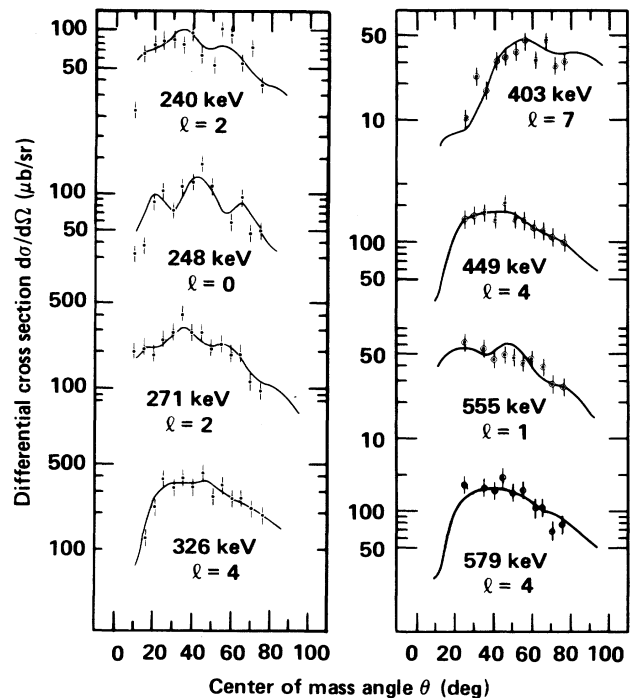


FIG. 4. Differential cross sections for selected levels populated by the reaction $^{230}\text{Th}(d,p)^{231}\text{Th}$ as a function of angle θ .

III. EXCITED LEVELS OF ^{231}Th

The thermal neutron capture reaction in a ^{230}Th target produces a capture state in ^{231}Th with spin and parity $\frac{1}{2}^+$. In the γ -ray cascade that follows capture, levels with low spin are populated with greatest intensity. In the present work, the experimental sensitivity was insufficient to detect γ rays populating most levels with $I = \frac{1}{2} - \frac{7}{2}$.

A first step in interpreting the capture- γ spectroscopic data was the construction of a model-independent level scheme based on the following principles: (a) Derivation of precise level energies using the Ritz combination principle (this technique becomes more powerful as the precision of the γ -ray energy determination increases; the precise results obtained with the curved-crystal spectrometers are an important feature in the success of the ^{231}Th level scheme derived here). (b) Use of experimental transition multiplicities or, if not determined as in cases of weak lines, the assumption that uncharacterized transitions are predominantly either $E1$, $E2$, or $M1$, plus intensity considerations, to limit possible spin and parity values; it was assumed that the spins and parities of the ground state $K^\pi = \frac{5}{2}^+$ band and the 186 keV $K^\pi = \frac{5}{2}^-$ band are well established; levels with $I > \frac{9}{2}$ are not expected to be observed via secondary γ lines. (c) Determination of $I^\pi = \frac{1}{2}^\pm, \frac{3}{2}^\pm$ levels from average resonance and thermal neutron capture data; levels below 800 keV not observed by ARC were assumed to have $I \geq \frac{5}{2}$. (d) Independent confirmation of a level's existence from α

TABLE IV. Differential cross sections for the $^{230}\text{Th}(d,p)^{231}\text{Th}$ reaction; $E_d = 20$ MeV.

E_{level}^a (keV)	Proposed config. assign. ^b	$d\sigma/d\Omega$ ($\mu\text{b}/\text{sr}$)													
		10°	15°	20°	25°	30°	35°	40°	45°	50°	55°	60°	65°	70°	75°
94(3)	$\frac{9}{2}^+, \frac{5}{2}^+ [633]$					12	8	9	10	8	9	5	6	6	7
162(2)	$\frac{11}{2}^+, \frac{5}{2}^+ [633]$		18	8	8	12	18	26	26	18	20	19	23	17	14
186(2)	$\frac{5}{2}^-, \frac{5}{2}^+ [752]$				3			9		13	3			2	2
205(3)	$\frac{7}{2}^-, \frac{5}{2}^+ [752]$							5			3	2			5
225(3)	$\frac{3}{2}^+, \frac{3}{2}^+ [631]$	5	4	9	6	5	5	10			7				5
240(1)	$\frac{5}{2}^+, \frac{3}{2}^+ [631]$	23	66	77	82	88	80	97	63	51	105	93	57	78	37
248(1)	$\frac{1}{2}^+, \frac{1}{2}^+ [631]$	32	38	85	103	72	116	126	181	116	57	58	84	48	50
271(1)	$\frac{3}{2}^+, \frac{1}{2}^+ [631]$	203	221	198	256	297	420	298	303	213	244	198	194	114	101
280(3)	$\frac{11}{2}^-, \frac{5}{2}^+ [752]$		28	48	65	36	52	36	41	39	35	44	22	39	38
301(1)	$\frac{5}{2}^+, \frac{1}{2}^+ [631]$		15	24	27	36	41	29	30	21	24	24	20	15	11
317(1)	$\frac{5}{2}^+, \frac{5}{2}^+ [622]$			13	30	32	19	23	18	24	22	55	20	48	13
326(1)	$\frac{9}{2}^+, \frac{3}{2}^+ [631]$		126	230	386	330	397	340	442	290	352	271	268	216	195
335(2)	$\frac{13}{2}^-, \frac{5}{2}^+ [752]$			12	32	33	25	27	42	84	21	28	23	24	24
351(1)	$\frac{7}{2}^+, \frac{1}{2}^+ [631]$		12	31	37	43	34	32	37	28	23	17	17	17	14
380(1)	$\frac{7}{2}^+, \frac{5}{2}^+ [622]$			22	34	31	16	24	25	13	14	16	12	10	10
403(2)	$\frac{15}{2}^-, \frac{5}{2}^+ [752]$			10	23	23	18	32	34	39	47	32	46	30	32
449(1)	$\frac{9}{2}^+, \frac{5}{2}^+ [622]$			156	165	165	179	156	204	160	152	133	131	111	105
465(2)	$\frac{11}{2}^+, \frac{1}{2}^+ [631]$					22	14	16	21	22	27	21	32	20	20
490(3)	$\frac{11}{2}^-, \frac{7}{2}^+ [743] \& \frac{11}{2}^+, \frac{5}{2}^+ [622]$				15	10	18	21	21	11	18	22	24	21	22
530(3)	$\frac{1}{2}^-, \frac{1}{2}^+ [501]$				28			6	5	12		5	14	11	
555(1)					62		57	45	50	45	43	43	39	27	26
568(3)				13				10	7	17	10		7	14	11
579(1)				170			158	148	192	146	152	105	110	68	78
592(2)	$\frac{3}{2}^-, \frac{3}{2}^+ [761] \& \frac{3}{2}^-, \frac{1}{2}^+ [501]$		35				39	38	38	35	33	32	35	11	14
622(3)	$\frac{3}{2}^-, \frac{3}{2}^+ [631] \times 0^- \& \frac{5}{2}^-, \frac{5}{2}^+ [752] \times 0^+$							12	16	16	7		12	4	5
653(3)	$\frac{7}{2}^-, \frac{3}{2}^+ [761]$						14	12	20	13	20	18	1	9	8
684(2)	$\frac{5}{2}^-, \frac{5}{2}^+ [503]$						14	8	31	20	15	18	21	12	10
704(2)	$\frac{15}{2}^-, \frac{7}{2}^+ [743]$						11	16	24	19	16	22	24	11	12
724(3)	$\frac{7}{2}^-, \frac{1}{2}^+ [770]$						12	16	8	9	6	6	6	10	7

TABLE IV. (Continued).

E_{level}^a (keV)	Proposed config. assign. ^b	10°	15°	20°	25°	30°	35°	40°	45°	50°	55°	60°	65°	70°	75°
745(3)							12	18	14	13	18	21	10	6	5
802(2)							27	30	40	36	21	23	22	20	15
813(3)							8	24	27	17	14	8	16	17	13
837(3)	$\frac{3}{2}^+, \frac{1}{2}[631]\times 0^+$						29	29	32	15	20	23	21	17	18
867(2)							58	50	56	44	47	53	43	32	35
881(2)							53	45	47	25	32	30	30	23	19
893(2)	$\frac{7}{2}^+, \frac{1}{2}[640]\&\frac{1}{2}[631]\times 0^+$						30	22	26	18	18	25	19	10	7
947(3)			15				18	19	13	15	11	13	10	12	9
965(5)	$\frac{9}{2}^+, \frac{1}{2}[640]\&\frac{1}{2}[631]\times 0^+$						18	15	15	21	16	16	16	22	13
981(3)					7		18	7	15	9	4	12	11	7	8
1002(3)								19	19	26	10	19	16	24	8
1016(3)				30	42			45	55	43	35	27	33	33	21
1058(2)				30	84			97	109	71	21	69	41	34	19
1067(2)				51	18			24	37	47	94	34	62	31	28
1087(3)				29	43			24	20	11	26	22	26	13	5
1101(2)				33	22			73	83	54	62	49	48	34	33
1114(3)					22			25	35	19	35	13	17	16	12
1162(2)					22			27	37	32	38	29	31	18	7
1175(2)					17			17	49	26	17	23	20	22	24
1202(2)					121			76	76	73	67	40	56	27	34
1213(2)					46			117	117	84	89	75	49	54	47
1226(2)					25			29	29	28	11	31	9	7	17
1282(3)								44	44	65	31	40	36	29	28
1329(2)		33						38	38	37	21	33	19	27	35
1339(2)		71						122	122	129	92	94	84	74	64
1350(2)		70						105	105	107	93	91	83	58	61
1366(4)								61	61	43	71	32	28	18	21
1376(5)								24	24	24		31	22	14	17
1390(5)								48	48	48	16	28	28	21	18
1404(5)		24	93			90	208	100	100	126	54	88	93	44	35
1414(5)			82				39			59	110	89	62	82	48

^aUncertainty shown in parentheses.^bConfiguration assignments are from last column of Table VI; discussion of assignments is given in Sec. IV.

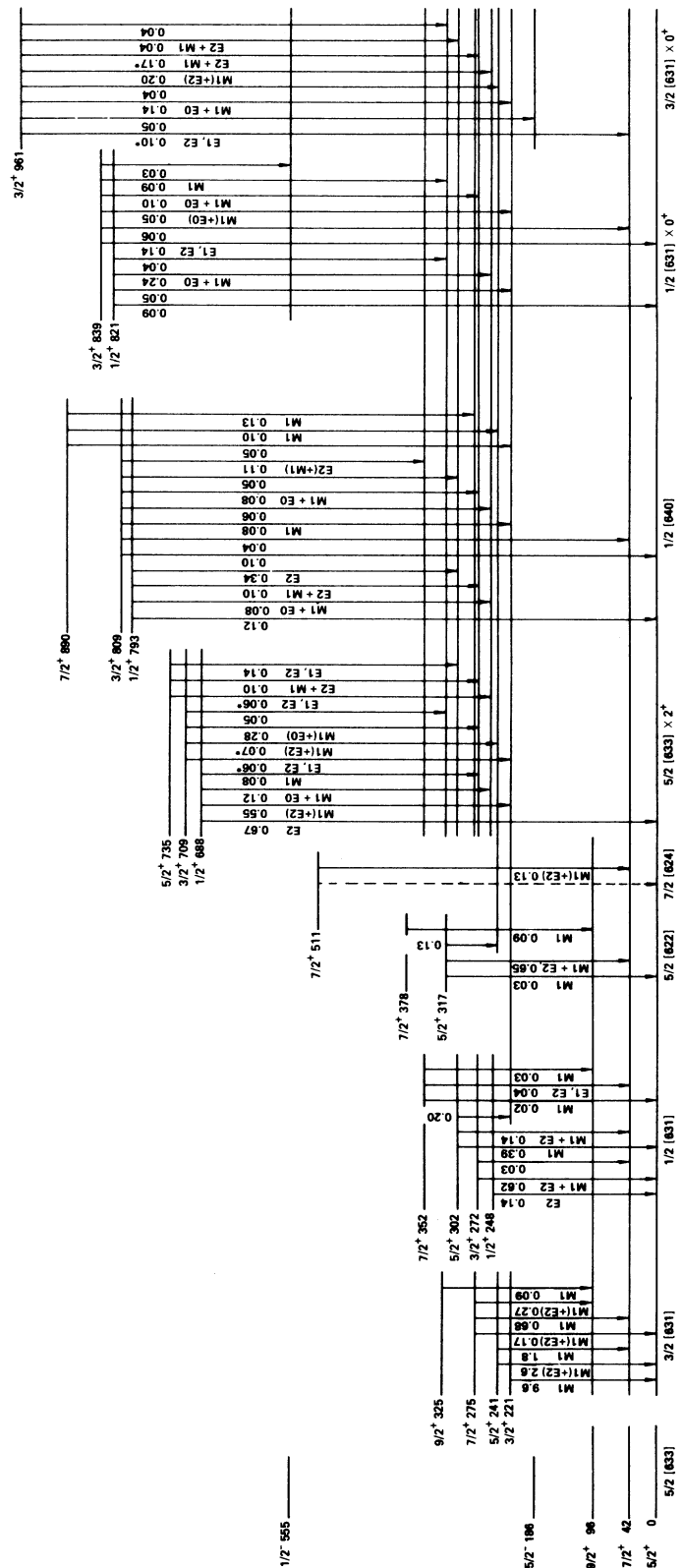


FIG. 5. Positive-parity levels in ^{231}Th assigned to rotational bands and depopulating transitions. Estimated confidence in configuration assignments: well established— $\frac{5}{2}^+ [633]$, $\frac{3}{2}^+ [631]$, $\frac{1}{2}^+ [631]$; probable— $\frac{5}{2}^+ [622]$, $\frac{5}{2}^+ [633] \times 2^+$, $\frac{1}{2}^+ [631] \times 0^+$; plausible— $\frac{7}{2}^+ [624]$, $\frac{1}{2}^+ [640]$, $\frac{3}{2}^+ [631] \times 0^+$.

TABLE V. Gamma decay of levels in ^{231}Th .

E_i (keV)	$I_i^{\pi a}$	E_f (keV)	$I_f^{\pi a}$	E_γ (keV)	I_γ (per 100 n)	Multipol. ^b	E_i (keV)	$I_i^{\pi a}$	E_f (keV)	$I_f^{\pi a}$	E_γ (keV)	I_γ (per 100 n)	Multipol. ^b
186	$\frac{5}{2}^-$	0	$\frac{5}{2}^+$	186	18.0	E1	352	$\frac{7}{2}^+$	0	$\frac{5}{2}^+$	352	0.02	M1
		42	$\frac{7}{2}^+$	144	3.2	E1			42	$\frac{7}{2}^+$	310	0.04	$E1, E2^*$
205	$\frac{7}{2}^-$	0	$\frac{5}{2}^+$	205	0.35	$E1, E2^*$			96	$\frac{9}{2}^+$	255	0.03	M1
		42	$\frac{7}{2}^+$	163	0.41	$E1, E2^*$	378	$\frac{7}{2}^+$	96	$\frac{9}{2}^+$	281	0.09	M1
221	$\frac{3}{2}^+$	0	$\frac{5}{2}^+$	221	9.59	M1	388	$\frac{7}{2}^-$	186	$\frac{5}{2}^-$	202	0.21	M1
241	$\frac{5}{2}^+$	0	$\frac{5}{2}^+$	241	2.6	$M1(+E2)$			205	$\frac{7}{2}^-$	183	0.08	
		42	$\frac{7}{2}^+$	199	1.8	M1	511	$\frac{7}{2}^+$	42	$\frac{7}{2}^+$	469	0.13	$M1(+E2)$
248	$\frac{1}{2}^+$	0	$\frac{5}{2}^+$	248	0.14	E2	555	$\frac{1}{2}^-$	186	$\frac{5}{2}^+$	369	0.77	E2
272	$\frac{3}{2}^+$	0	$\frac{5}{2}^+$	272	0.62	$M1+E2$			248	$\frac{1}{2}^+$	307	1.63	E1
		42	$\frac{7}{2}^+$	230	0.03		591	$\frac{3}{2}^-$	272	$\frac{3}{2}^+$	282	2.15	E1
275	$\frac{7}{2}^+$	0	$\frac{5}{2}^+$	275	0.17	$M1(+E2)$			186	$\frac{5}{2}^-$	405	1.00	$E2+M1$
		42	$\frac{7}{2}^+$	233	0.68	M1			205	$\frac{7}{2}^-$	386	0.25	$E1, E2^*$
		96	$\frac{9}{2}^+$	179	0.27	$M1(+E2)$	594	$\frac{3}{2}^-$	302	$\frac{5}{2}^+$	289	0.03	
302	$\frac{5}{2}^+$	0	$\frac{5}{2}^+$	302	0.39	M1			186	$\frac{5}{2}^-$	408	1.56	E2
		42	$\frac{7}{2}^+$	260	0.14	$M1+E2$	596	$\frac{5}{2}^-$	221	$\frac{3}{2}^+$	372	0.64	E1
		221	$\frac{3}{2}^+$	80	0.20				186	$\frac{5}{2}^-$	410	0.08	M1
317	$\frac{5}{2}^+$	0	$\frac{5}{2}^+$	317	0.03	M1			205	$\frac{7}{2}^-$	391	0.17	$M1+E2$
		42	$\frac{7}{2}^+$	275	0.65	$M1+E2$			221	$\frac{3}{2}^+$	375	0.06	$E1, E2^*$
		241	$\frac{5}{2}^+$	76	0.13		620	$\frac{3}{2}^-$	272	$\frac{3}{2}^+$	324	0.27	$E1, E2^*$
325	$\frac{9}{2}^+$	96	$\frac{9}{2}^+$	229	0.09	M1			352	$\frac{7}{2}^+$	244	0.05	$E1, E2^*$
									186	$\frac{5}{2}^-$	434	0.20	M1
									221	$\frac{3}{2}^+$	398	0.07	$E1, E2^*$
									302	$\frac{5}{2}^+$	318	0.02	
									317	$\frac{5}{2}^+$	303	0.05	$E1, E2^*$

TABLE V. (Continued).

E_i (keV)	$I_i^{\pi a}$	E_f (keV)	$I_f^{\pi a}$	E_γ (keV)	I_γ (per 100 n)	Multipol. ^b	E_i (keV)	$I_i^{\pi a}$	E_f (keV)	$I_f^{\pi a}$	E_γ (keV)	I_γ (per 100 n)	Multipol. ^b
624	$\frac{5}{2}^-$	186	$\frac{7}{2}^-$	438	0.01	M1+E0	720	$\frac{7}{2}^-$	186	$\frac{5}{2}^-$	535	0.07	M1
		205	$\frac{7}{2}^-$	419	0.01	D			205	$\frac{7}{2}^-$	515	0.47	M1+E2
629	$\frac{5}{2}^-$	0	$\frac{5}{2}^+$	629	0.09				275	$\frac{7}{2}^+$	445	0.08	E1,E2*
		186	$\frac{5}{2}^-$	444	0.94	M1(+E2)	735	$\frac{5}{2}^+$	248	$\frac{1}{2}^+$	488	0.06	E1,E2*
		205	$\frac{7}{2}^-$	424	0.36	M1+E2			272	$\frac{3}{2}^+$	463	0.10	E2+M1
634	$\frac{7}{2}^-$	186	$\frac{5}{2}^-$	448	0.02				302	$\frac{5}{2}^+$	434	0.14	E1,E2*
		205	$\frac{7}{2}^-$	429	0.02	M1+E0	793	$\frac{1}{2}^+$	0	$\frac{5}{2}^+$	793	0.12	
656	$\frac{7}{2}^-$	186	$\frac{5}{2}^-$	470	0.04				248	$\frac{1}{2}^+$	545	0.08	M1+E0
		237	$\frac{9}{2}^-$	419	0.05	M1			272	$\frac{3}{2}^+$	521	0.10	E2+M1
684	$\frac{5}{2}^-$	186	$\frac{5}{2}^-$	499	1.25	M1			302	$\frac{5}{2}^+$	491	0.34	E2
		205	$\frac{7}{2}^-$	479	0.12	E2	809	$\frac{3}{2}^+$	0	$\frac{5}{2}^+$	808	0.10	
688	$\frac{1}{2}^+$	0	$\frac{5}{2}^+$	688	0.67	E2			42	$\frac{7}{2}^+$	767	0.04	
		221	$\frac{3}{2}^+$	466	0.55	M1(+E2)			221	$\frac{3}{2}^+$	587	0.08	M1
		248	$\frac{1}{2}^+$	440	0.12	M1+E0			248	$\frac{1}{2}^+$	561	0.06	
		272	$\frac{3}{2}^+$	415	0.08	M1			272	$\frac{3}{2}^+$	536	0.08	M1+E0
709	$\frac{3}{2}^+$	221	$\frac{3}{2}^+$	488	0.06	E1,E2*			302	$\frac{5}{2}^+$	507	0.05	
		241	$\frac{5}{2}^+$	468	0.07	M1(+E2)	821	$\frac{1}{2}^+$	352	$\frac{7}{2}^+$	457	0.01	E2(+M1)
		272	$\frac{3}{2}^+$	437	0.28	M1(+E0)			0	$\frac{5}{2}^+$	820	0.09	
		317	$\frac{5}{2}^+$	392	0.05				221	$\frac{3}{2}^+$	599	0.05	
714	$\frac{3}{2}^-$	186	$\frac{5}{2}^-$	528	0.70	M1	833	$\frac{1}{2}^-$	221	$\frac{3}{2}^+$	612	0.09	
		272	$\frac{3}{2}^+$	442	0.03				248	$\frac{1}{2}^+$	586	0.11	
		388	$\frac{7}{2}^-$	326	0.17				555	$\frac{1}{2}^-$	279	0.03	
									594	$\frac{3}{2}^-$	240	0.40	M1

TABLE V. (Continued).

E_i (keV)	$I_i^{p.a}$	E_f (keV)	$I_f^{p.a}$	E_γ (keV)	I_γ (per 100 n)	Multipol. ^b	E_i (keV)	$I_i^{p.a}$	E_f (keV)	$I_f^{p.a}$	E_γ (keV)	I_γ (per 100 n)	Multipol. ^b
839	$\frac{3}{2}^+$	0	$\frac{5}{2}^+$	839	0.14	$E1, E2^*$			186	$\frac{5}{2}^-$	775	0.05	
		42	$\frac{7}{2}^+$	798	0.06				221	$\frac{3}{2}^+$	739	0.14	$M1+E0$
		221	$\frac{3}{2}^+$	618	0.05	$M1(+E0)$			241	$\frac{5}{2}^+$	720	0.04	
		272	$\frac{3}{2}^+$	567	0.10	$M1+E0$			248	$\frac{1}{2}^+$	713	0.20	$M1(+E2)$
		317	$\frac{5}{2}^+$	522	0.09	$M1$			272	$\frac{3}{2}^+$	689	0.17	$E2+M1$
		555	$\frac{1}{2}^-$	285	0.03				302	$\frac{5}{2}^+$	659	0.04	$E2+M1$
									317	$\frac{5}{2}^+$	644	0.04	
867	$\frac{5}{2}^-$	186	$\frac{5}{2}^-$	681	0.10	$E2+M1$	1004	$\frac{3}{2}^+$	241	$\frac{5}{2}^+$	763	0.16	$M1$
		237	$\frac{7}{2}^-$	630	0.06	$E2$			378	$\frac{7}{2}^+$	627	0.06	
		388	$\frac{7}{2}^-$	479	0.12	$E2$	D						
876	$\frac{3}{2}^-$	0	$\frac{5}{2}^+$	876	0.13		1021	$\frac{3}{2}^-$	186	$\frac{5}{2}^-$	835	0.14	$M1$
		555	$\frac{1}{2}^-$	321	0.10	$M1(+E2)$			221	$\frac{3}{2}^+$	799	0.09	
		620	$\frac{3}{2}^-$	256	0.03	$M1$			248	$\frac{1}{2}^+$	773	0.05	
890	$\frac{7}{2}^+$	221	$\frac{7}{2}^+$	669	0.05				594	$\frac{3}{2}^-$	427	0.10	$M1$
		241	$\frac{5}{2}^+$	649	0.10	$M1$			684	$\frac{5}{2}^-$	336	0.04	$M1$
		275	$\frac{7}{2}^+$	615	0.13	$M1$							
915	$\frac{5}{2}^-$	0	$\frac{5}{2}^+$	915	0.15		1056	$\frac{3}{2}^+$	42	$\frac{7}{2}^+$	1014	0.41	$E1, E2^*$
		186	$\frac{5}{2}^-$	729	0.08				221	$\frac{3}{2}^+$	835	0.14	$M1$
		237	$\frac{9}{2}^-$	678	0.03				248	$\frac{1}{2}^+$	809	0.09	
936	$\frac{5}{2}^-$	0	$\frac{5}{2}^+$	674	0.05				272	$\frac{3}{2}^+$	784	0.11	
		186	$\frac{5}{2}^-$	936	0.23		1066	$(\frac{5}{2})^+$	0	$\frac{5}{2}^+$	1066	0.08	
		317	$\frac{5}{2}^+$	751	0.23	$M1$			42	$\frac{7}{2}^+$	1025	0.07	
				619	0.06				221	$\frac{3}{2}^+$	845	0.04	
		388	$\frac{7}{2}^-$	548	0.08	$E2+M1$			317	$\frac{5}{2}^+$	749	0.10	$M1$
		594	$\frac{3}{2}^-$	343	0.03	$M1$	1074	$\frac{3}{2}^-$	378	$\frac{7}{2}^+$	689	0.17	$E2+M1$
961	$\frac{3}{2}^+$	42	$\frac{7}{2}^+$	919	0.10	$E1, E2^*$			186	$\frac{5}{2}^-$	888	0.07	
									317	$\frac{5}{2}^+$	757	0.05	
									591	$\frac{3}{2}^-$	484	0.06	$M1+E2$

TABLE V. (Continued).

E_i (keV)	$I_i^{\pi a}$	E_f (keV)	$I_f^{\pi a}$	E_γ (keV)	I_γ (per 100 n)	Multipol. ^b	E_i (keV)	$I_i^{\pi a}$	E_f (keV)	$I_f^{\pi a}$	E_γ (keV)	I_γ (per 100 n)	Multipol. ^b		
1081	$\frac{1}{2}^-$	555	$\frac{1}{2}^-$	527	0.03	M1	1133	$(\frac{1}{2}^+, \frac{3}{2}^+, \frac{5}{2}^+)$	248	$\frac{1}{2}^+$	886	0.06			
	$\frac{3}{2}^-$	591	$\frac{3}{2}^-$	491	0.06	M1			272	$\frac{3}{2}^+$	862	0.04			
		594	$\frac{3}{2}^-$	488	0.06	$E1, E2^*$			T	317	$\frac{5}{2}^+$	817	0.07		D
1087	$\frac{5}{2}^+$	272	$\frac{3}{2}^+$	815	0.15	$E1, E2^*$	1160	$\frac{1}{2}^-, \frac{3}{2}^-$	186	$\frac{5}{2}^-$	974	0.06			
		275	$\frac{7}{2}^+$	811	0.38	E2			241	$\frac{5}{2}^+$	919	0.10		$E1, E2^*$	
		302	$\frac{5}{2}^+$	785	0.10				T	714	$\frac{3}{2}^-$	446	0.14		$E2(+M1)$
		378	$\frac{7}{2}^+$	709	0.56	$E2+M1$									
		594	$\frac{3}{2}^-$	493	0.05	$E1, E2^*$				1173	$\frac{3}{2}^-$	388	$\frac{7}{2}^-$	785	0.10
1102	$\frac{3}{2}^-$	241	$\frac{5}{2}^+$	862	0.04				629	$\frac{5}{2}^-$	544	0.03	M1		
		317	$\frac{5}{2}^+$	785	0.10				684	$\frac{5}{2}^-$	489	0.02			
		620	$\frac{3}{2}^-$	483	0.03				714	$\frac{3}{2}^-$	459	0.05	M1		
		634	$\frac{7}{2}^-$	468	0.08	$M1(+E2)$	D								
		684	$\frac{5}{2}^-$	418	0.05	M1									
		714	$\frac{3}{2}^-$	388	0.08										

^aSpin and parity values listed are for the assigned Nilsson configuration (see Table VI for details).

^bThe notation for the multipolarity listing is the same as in Table I. Following this, the entries D and T denote transitions that are multiply placed in the level scheme (D denotes twice, T thrice).

TABLE VI. Energy levels in ^{231}Th .

Level energy ^a (keV)	Model independent spin and parity ^b	Energy (prim. γ) (keV)	Tot. pop. (per 100 cap.)	Tot. depop.	Energy (d,p) (keV)	Other experimental observations ^c	Confid. ^d	Config. assign.
0.0	$\frac{5}{2}^+$		77			TC dt α	A	$\frac{5}{2}^+, \frac{5}{2} [633]$
41.952(2)	$\frac{7}{2}^+$		15.6			dt α	A	$\frac{7}{2}^+, \frac{5}{2} [633]$
96.129(3)	$\frac{9}{2}^+$		0.9		94(2)	dp dt α	A	$\frac{9}{2}^+, \frac{5}{2} [633]$
161.94(4) ^e	$\frac{11}{2}^+$				162(2)	dp dt α	A	$\frac{11}{2}^+, \frac{5}{2} [633]$
185.715(2)	$\frac{5}{2}^-$		10.3	22.7	186(2)	dp dt α	A	$\frac{5}{2}^-, \frac{5}{2} [752]$
205.310(2)	$\frac{7}{2}^-$		1.7	0.8	205(3)	dp α	A	$\frac{7}{2}^-, \frac{5}{2} [752]$
221.398(2)	$\frac{3}{2}^+$	221.3(2)	2.5	29.5	225(3)	TC RC dp α	A	$\frac{3}{2}^+, \frac{3}{2} [631]$
236.954(31)	$\frac{9}{2}^-$		0.2			α	A	$\frac{9}{2}^-, \frac{5}{2} [752]$
240.881(2)	$\frac{5}{2}^+, \frac{7}{2}^+$		0.7	14	240(1)	dp dt $h\alpha\alpha$	A	$\frac{5}{2}^+, \frac{3}{2} [631]$
247.583(2)	$\frac{1}{2}^+, \frac{3}{2}^+$	247.8(4)	2.9	0.2	248(1)	TC RC dp α	A	$\frac{1}{2}^+, \frac{1}{2} [631]$
272.180(2)	$\frac{3}{2}^+$	272.1(1)	4.2	1.2	271(1)	TC RC dp dt α	A	$\frac{3}{2}^+, \frac{1}{2} [631]$
275.425(2)	$\frac{7}{2}^+$		0.6	2.6		α	A	$\frac{7}{2}^+, \frac{3}{2} [631]$
277.8(2) ^e					280(3)	dp dt $h\alpha\alpha$	B	$\frac{11}{2}^-, \frac{5}{2} [752]$
301.744(2)	$\frac{5}{2}^+, \frac{7}{2}^+$		0.7	1.3	301(1)	dp dt α	A	$\frac{5}{2}^+, \frac{1}{2} [631]$
317.082(2)	$\frac{5}{2}^+$		1.7	1.3	317(1)	dp α	B	$\frac{5}{2}^+, \frac{5}{2} [622]$
324.913(7)	$\frac{7}{2}^+, \frac{9}{2}^+, \frac{11}{2}^+$			0.1	326(1)	dp dt $h\alpha\alpha$	A	$\frac{9}{2}^+, \frac{3}{2} [631]$
335(2)					335(2)	dp α	B	$\frac{13}{2}^-, \frac{5}{2} [752]$
351.511(6)	$\frac{7}{2}^+$		0.2	0.2	351(1)	dp dt α	A	$\frac{7}{2}^+, \frac{1}{2} [631]$
377.577(8)	$\frac{7}{2}^+, \frac{9}{2}^+$		0.8	0.2	380(1)	dp dt α	B	$\frac{7}{2}^+, \frac{5}{2} [622]$
385.69(5) ^e						α	C	$\frac{11}{2}^+, \frac{3}{2} [631]$
387.827(2)	$\frac{5}{2}^-, \frac{7}{2}^-$		0.6	0.8		α	A	$\frac{7}{2}^-, \frac{7}{2} [743]$
403(2)					403(2)	dp dt $h\alpha$	B	$\frac{15}{2}^-, \frac{5}{2} [752]$
449(1)					449(1)	dp dt α	C	$\frac{9}{2}^+, \frac{5}{2} [622]$
452.18(2) ^e						α	A	$\frac{9}{2}^-, \frac{7}{2} [743]$
490(3)					490(3)	dp dt α	C	$\frac{11}{2}^+, \frac{1}{2} [631]$
510.897(10) ^f	$\frac{7}{2}^+$			0.1		α	C	$\frac{7}{2}^+, \frac{7}{2} [624]$
530(3)					530(3)	dp α	C	$\frac{11}{2}^-, \frac{7}{2} [743] \& \frac{11}{2}^+, \frac{5}{2} [622]$
554.651(2)	$\frac{1}{2}^-, \frac{3}{2}^-$	554.7(2)	0.2	7.1	555(1)	TC RC dp dt β	A	$\frac{1}{2}^-, \frac{1}{2} [501]$
580(1)					579(1)	dp dt $h\alpha$	C	$\frac{9}{2}^+, \frac{7}{2} [624]$
590.838(2)	$\frac{3}{2}^-$	591.0(1)	0.1	1.5	592(2)	TC RC dp α	A	$\frac{3}{2}^-, \frac{3}{2} [761]$
593.617(2)	$\frac{1}{2}^-, \frac{3}{2}^-$	594.3(3)	1.5	2.3	592(2)	TC RC dp dt β	A	$\frac{3}{2}^-, \frac{1}{2} [501]$
595.974(2)	$\frac{5}{2}^-$			0.7		α	B	$\frac{5}{2}^-, \frac{1}{2} [501]$
619.638(4)	$\frac{3}{2}^-$	619.8(2)	0.1	0.4	622(3)	(TC) RC dp dt α	D	$\frac{3}{2}^-, \frac{3}{2} [631] \times 0^-$
623.937(18) ^f	$\frac{5}{2}^-$			0.1	622(3)	dp dt α	D	$\frac{5}{2}^-, \frac{5}{2} [752] \times 0^+$
629.342(2)	$\frac{5}{2}^-, \frac{7}{2}^-$			1.7		α	B	$\frac{5}{2}^-, \frac{3}{2} [761]$
634.044(13) ^f	$\frac{7}{2}^-$		0.1	0.1		α	D	$\frac{7}{2}^-, \frac{5}{2} [752] \times 0^+$

TABLE IV. (Continued).

Level energy ^a (keV)	Model independent spin and parity ^b	Energy (prim. γ) (keV)	Tot. pop. (per 100 cap.)	Tot. depop.	Energy (d,p) (keV)	Other experimental observations ^c	Confid. ^d	Config. assign.
655.981(25) ^f	$\frac{7}{2}^-, \frac{9}{2}^-$			0.1	653(3)	dp	C	$\frac{7}{2}^-, \frac{3}{2}^-[761]$
684.490(2)	$\frac{3}{2}^-, \frac{5}{2}^-, \frac{7}{2}^-$	685.6(5)	0.2	1.6	685(2)	RC dp dt	D	$\frac{5}{2}^-, \frac{5}{2}^-[503]$
687.631(3)	$\frac{1}{2}^+, \frac{3}{2}^+$		0.2	1.6		(dt)	B	$\frac{1}{2}^+(\frac{1}{2}[631]\times 0^+ \& \frac{5}{2}[633]\times 2^+)$
704(2)					704(2)	dp dt	B	$\frac{15}{2}^-, \frac{7}{2}^-[743]$
709.099(4)	$\frac{3}{2}^+, \frac{5}{2}^+$			0.6		dt	B	$\frac{3}{2}^+(\frac{1}{2}[631]\times 0^+ \& \frac{5}{2}[633]\times 2^+)$
713.753(2)	$\frac{3}{2}^-$	713.6(2)	0.3	1.5		TC RC	C	$\frac{3}{2}^-, \frac{1}{2}^-[770]$
720.298(5)	$\frac{5}{2}^-, \frac{7}{2}^-$			0.8	724(3)	dp dt	C	$\frac{7}{2}^-, \frac{1}{2}^-[770]$
735.263(6)	$\frac{5}{2}^+$			0.3			C	$\frac{5}{2}^+(\frac{1}{2}[631]\times 0^+ \& \frac{5}{2}[633]\times 2^+)$
793.026(4)	$\frac{1}{2}^+, \frac{3}{2}^+$	794.2(1)		0.6		RC	C	$\frac{1}{2}^+(\frac{1}{2}[640]\& \frac{5}{2}[631]\times 0^+)$
808.507(8)	$\frac{3}{2}^+$			0.6			C	$\frac{3}{2}^+(\frac{1}{2}[640]\& \frac{1}{2}^+[631]\times 0^+)$
813(2) ^e						dt $h\alpha$	C	$\frac{15}{2}^-, \frac{1}{2}^-[770]$
820.544(7)	$\frac{1}{2}^+, \frac{3}{2}^+$	820.9(2)		0.6		TC	B	$\frac{1}{2}^+, \frac{1}{2}^-[631]\times 0^+$
833.168(4)	$\frac{1}{2}^-, \frac{3}{2}^-$	833.3(2)		1.4		TC RC (dp)	C	$\frac{1}{2}^-, \frac{1}{2}^-[770]$
839.304(8)	$\frac{3}{2}^+$	839.4(2)		0.5	837(3)	TC RC (dp) dt	B	$\frac{3}{2}^+, \frac{1}{2}^-[631]\times 0^+$
854(4) ^e						dt	C	$\frac{5}{2}^+(\frac{1}{2}[640]\& \frac{1}{2}[631]\times 0^+)$
875.549(4)	$\frac{3}{2}^-$	875.5(2)		0.3		TC RC dt	C	$\frac{3}{2}^-, \frac{3}{2}^-[501]$
889.998(12)	$\frac{5}{2}^+, \frac{7}{2}^+$		0.1	0.7	893(2)	dp dt	C	$\frac{7}{2}^+(\frac{1}{2}[640]\& \frac{1}{2}[631]\times 0^+)$
914.904(40)	$\frac{5}{2}^-, \frac{7}{2}^-$			0.3		dt $h\alpha$	C	$\frac{5}{2}^-, \frac{3}{2}^-[501]$
960.807(11)	$\frac{3}{2}^+$	960.7(2)		0.8		TC (RC) dt	C	$\frac{3}{2}^+, \frac{3}{2}^-[631]\times 0^+$
970(4)					965(5)	dp dt	C	$\frac{9}{2}^+(\frac{1}{2}[640]\& \frac{1}{2}[631]\times 0^+)$
1004.236(20)	$\frac{3}{2}^+$	1004.0(1)		0.2	1002(3)	TC RC dp dt		
1020.728(5)	$\frac{3}{2}^-$	1021.3(2)		0.5		TC RC dp dt		
1033(4) ^e						dt	C	$\frac{11}{2}^+(\frac{1}{2}[640]\& \frac{1}{2}[631]\times 0^+)$
1056.30(3)	$\frac{3}{2}^+$	1055.7(1)		0.8	1058(2)	TC dp		
1066.19(2)	$(\frac{5}{2}^+)$			0.5	1067(2)	dp		
1074.35(2)	$\frac{3}{2}^-$	1075.1(8)		0.2		RC		
1081.33(2)	$\frac{1}{2}^-, \frac{3}{2}^-$	1081.2(9)		0.2		RC		
1084(4) ^e						dt	C	$\frac{15}{2}^-, \frac{3}{2}^-[761]$
1086.812(10)	$\frac{5}{2}^+$			1.3	1087(3)	dp dt		
1102.25(1)	$\frac{3}{2}^-$	1103.3(4)		0.4	1101(2)	RC dp dt $h\alpha$		
1133.81(8)	$\frac{1}{2}^+, \frac{3}{2}^+, \frac{5}{2}^+$	1134(3)		0.8		(TC) RC		
1159.750(7)	$\frac{1}{2}^-, \frac{3}{2}^-$	1159.5(2)		0.3	1162(2)	TC RC dp		
1173.00(2)	$\frac{3}{2}^-$	1172.1(4)		0.2	1175(2)	TC RC dp		

^aEnergies obtained from a least squares fit of level energies to transition energies.

^bSee text (Sec. III, second paragraph) for explanation of method for making model independent spin and parity assignments.

^cTC denotes thermal neutron capture, RC denotes average resonance capture, dp denotes (d,p) reaction, dt denotes (d,t) reaction, $h\alpha$ denotes ($^3\text{He},\alpha$) reaction, α denotes alpha decay, and β denotes beta decay.

^dEstimated confidence in evidence for a level's configuration assignment: A denotes well established, B denotes probable, C denotes plausible, D denotes speculative.

^eListed energy taken from previous experimental determination.

^fBased on present evidence, existence of level considered tentative.

particle spectra, α or β decay γ rays, or single-nucleon transfer reactions (d,p), (d,t), and ($^3\text{He},\alpha$). Thus, the model-independent level scheme is based on proven physical concepts.

A level scheme consisting of 57 levels with configuration assignments and within which 157 transitions are placed was established from the present experimental data. The γ decay of 51 levels is given in Table V; also, depopulating transitions from those levels assigned to rotational bands are shown in Figs. 5 and 6. All levels assigned to ^{231}Th are listed in Table VI, along with a summary of the evidence for their existence. The model independent spin and parity assignments are given in column 2 of Table VI. The level energies and uncertainties in Table VI were determined from the present (n, γ) data and calculated from a least-squares fit of energy differences to the complete set of transition energies.³⁶ Also given in Table VI are the total *observed* transition strengths that populate or depopulate a given level. For many levels, but especially for certain low-lying ones, the population and depopulation strengths are quite different. This can be understood in terms of low-energy transitions (often having large conversion coefficients) that were not detected in the present study, even though the conversion electron spectrum was scanned to rather low energies. A few very intense transitions that follow ^{231}Th β decay apparently obscure those in question. Configuration assignments are given for most of the levels, along with an indication of the authors' confidence in the validity of the assignments (well established, probable, plausible, or speculative), in the last two columns of Table VI.

With the inclusion of primary transition in the level fit, an experimental neutron binding energy of 5118.13 ± 0.20 keV was determined for ^{231}Th . The major part of the uncertainty is due to the systematic error in the aluminum γ rays used for calibration. This result is consistent with the value 5120.5 ± 2.6 keV derived by Wapstra and Bos³⁷ from previous measurements.

In previous ^{235}U (Refs. 6–8) and ^{231}Ac (Refs. 10 and 11) decay studies, level energies were determined by use of Ge(Li)-detector spectroscopy for approximately 17 excited levels (arranged in six rotational bands) below 600 keV and with $I = < \frac{9}{2}$.

IV. ASSIGNMENT OF NILSSON ORBITALS TO ROTATIONAL BANDS

A. Level structure from model calculations

The arrangement of experimental levels into rotational bands and their assignment to Nilsson orbitals was guided by Nilsson model calculations for ^{231}Th and by comparison with observations for neighboring nuclei. Three such calculations, made previously by other authors who employed various potential forms (modified oscillator,³⁸ folded Yukawa,³⁸ and Woods-Saxon^{39,40}), are summarized in Table VII.

For the first seven configurations listed in Table VII (through $\frac{7}{2}^+[624]$) and for the $\frac{3}{2}^- [761]$ configuration, the calculated bandhead energies for a given configuration agree reasonably well (with energy spreads ranging up to

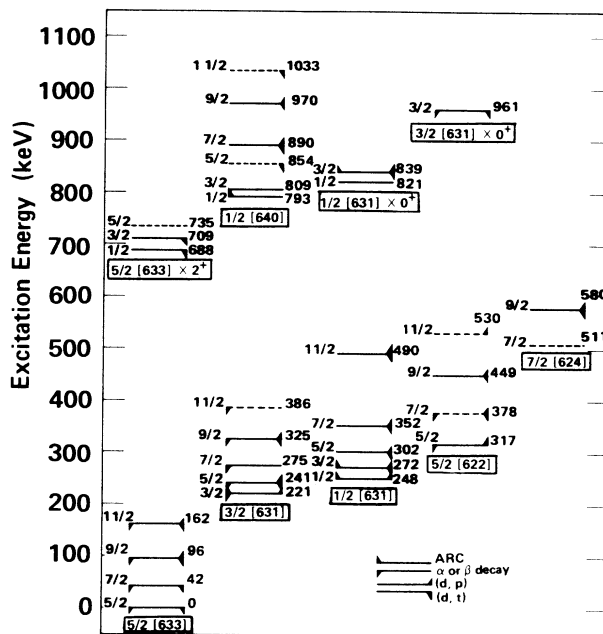


FIG. 7. Positive-parity levels in ^{231}Th assigned to rotational bands with Nilsson configuration assignments. Estimated confidence in configuration assignments: well established— $\frac{5}{2}^+[633]$, $\frac{3}{2}^+[631]$, $\frac{1}{2}^+[631]$; probable— $\frac{5}{2}^+[622]$, $\frac{5}{2}^+[633] \times 2^+$, $\frac{1}{2}^+[631] \times 0^+$; plausible— $\frac{7}{2}^+[624]$, $\frac{1}{2}^+[640]$, $\frac{3}{2}^+[631] \times 0^+$.

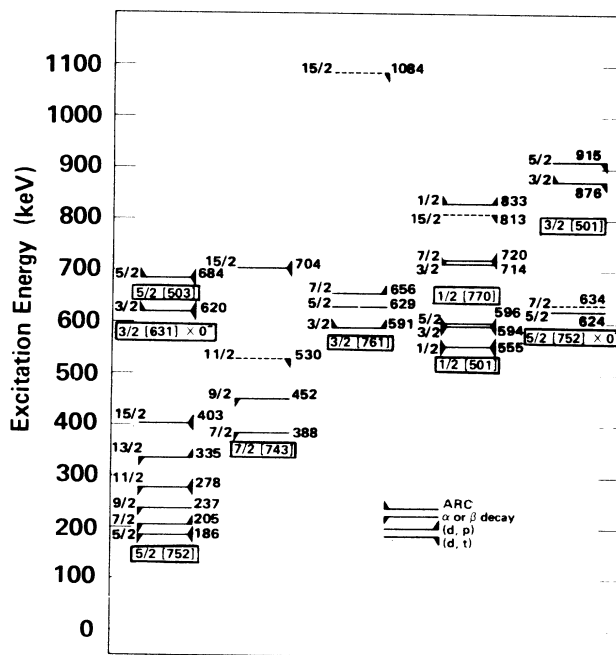


FIG. 8. Negative-parity levels in ^{231}Th assigned to rotational bands with Nilsson configuration assignments. Estimated confidence in configuration assignments; well established— $\frac{5}{2}^- [752]$, $\frac{7}{2}^- [743]$, $\frac{3}{2}^- [761]$, $\frac{1}{2}^- [501]$; plausible— $\frac{1}{2}^- [770]$, $\frac{3}{2}^- [501]$; speculative— $\frac{3}{2}^+[631] \times 0^-$, $\frac{5}{2}^- [752] \times 0^+$, $\frac{5}{2}^- [503]$.

TABLE VII. Experimental and calculated bandhead energies in ^{231}Th .

Config. ^a	Expt. energy (keV)	Decoupling parameters ^b		Calculated bandhead energies (keV)			Fraction indicated config. ^f	Other important components ^e	
		Expt.	Calc.	MO ^c	FY ^d	WS ^e			
$\frac{5}{2}^+[633]$	<i>A</i>	0.0		0	40	0	91%		
$\frac{5}{2}^- [752]$	<i>A</i>	185.7		20	0	220	92%		
$\frac{3}{2}^+[631]$	<i>A</i>	221.4		45	170	230	94%		
$\frac{1}{2}^+[631]$	<i>A</i>	247.6	+ 0.09	-0.39	250	380	240	72%	20% $\frac{1}{2}^+[631]\times 0^+$
$\frac{5}{2}^+[622]$	<i>B</i>	317.1		420	470	790	47%	46% $\frac{5}{2}^+[633]\times 0^+$	
$\frac{7}{2}^- [743]$	<i>A</i>	387.8		260	300	310	90%		
$\frac{7}{2}^+[624]$	<i>C</i>	510.9		520	830	560	80%		
$\frac{1}{2}^- [501]$	<i>A</i>	554.7	+ 0.93	+ 0.87	1075	400	670	47%	19% $\frac{1}{2}^- [752]\times 2^+$
$\frac{3}{2}^- [761]$	<i>A</i>	590.8		645	750	720	74%	10% $\frac{3}{2}^+[631]\times 0^-$	
$\frac{3}{2}^+[631]\times 0^-$	<i>D</i>	619.6							
$\frac{5}{2}^- [752]\times 0^+$	<i>D</i>	623.9				950	76%	13% $\frac{5}{2}^- [503]$	
$\frac{5}{2}^- [503]$	<i>D</i>	684.5		1420	960				
$\frac{5}{2}^+[633]\times 2^+$	<i>B</i>	687.6							
$\frac{1}{2}^+[640]$	<i>C</i>	793.0	-0.25	+ 0.16	1120	610	50%	30% $\frac{1}{2}^+[640]\times 0^+$	
$\frac{1}{2}^+[631]\times 0^+$	<i>B</i>	820.5							
$\frac{1}{2}^- [770]$	<i>C</i>	833.2	-7.2	-7.28	1150	1290	760	58%	10% $\frac{1}{2}^- [503]\times 2^+$
$\frac{3}{2}^- [501]$	<i>C</i>	875.5			1160				
$\frac{3}{2}^+[631]\times 0^+$	<i>C</i>	960.8				880	73%	18% $\frac{3}{2}^+[642]$	

^aNilsson configuration assignment and level of confidence: *A* denotes well established, *B* denotes probable, *C* denotes plausible, and *D* denotes speculative; discussion of these assignments is given in Sec. IV.

^bWoods-Saxon potential, $\epsilon_2=0.191$, $\epsilon_4=-0.044$, Ref. 40.

^cModified oscillator potential, $\epsilon_2=0.18$, $\epsilon_4=-0.05$, Ref. 38.

^dFolded Yukawa potential, $\epsilon_2=0.195$, $\epsilon_4=-0.05$, Ref. 38.

^eWoods-Saxon potential plus quadrupole phonon interaction, $\epsilon_2=0.19$, $\epsilon_4=-0.077$, Ref. 39.

^fBy "indicated configuration" we mean the configuration listed in column 1. The composition given in columns 8 and 9 is from Ref. 39.

370 keV). Thus, the sequence of these bandhead energies is predicted with only moderate ambiguity between potential forms. For configurations at higher energies, the deviations between the various calculations are somewhat larger. Calculated decoupling parameters for three of the $K = \frac{1}{2}$ bands are also listed in Table VII.

The results of the data interpretation are presented next; the rotational bands, their configuration assignments, and sources of supporting experimental evidence are summarized in Figs. 7 and 8.

B. Positive parity bands below 600 keV

1. $\frac{5}{2}^+[633]$: 0, 42, 96, and 162 keV

In previous studies of ^{235}U α decay⁴⁻⁸ and transfer reactions¹²⁻¹⁶ these levels have been established as rotational band members and given a $\frac{5}{2}^+[633]$ orbital assignment. The regular spacing of these levels indicates a $K = \frac{5}{2}$ band with rotational parameter $A=6.00$ keV.

2. $\frac{3}{2}^+[631]$: 221, 241, 275, 325, and 386 keV

These levels were established previously in ^{235}U α decay studies⁴⁻⁸ and were assigned to the $\frac{3}{2}^+[631]$ orbital.

Transitions that feed or depopulate the four lowest levels have been identified in this work. The observed level spacings indicate extreme compression of the band, a result of Coriolis mixing.

3. $\frac{1}{2}^+[631]$: 248, 272, 302, 352, and 490 keV

In previous studies this band was proposed to consist of levels at 248, 272, 317, 378, and 445 keV with a regular spin sequence $\frac{1}{2}^+ - \frac{3}{2}^+$. From the energy spacings of this proposed sequence, one derives a value of $A=8.6$ keV for the rotational parameter, which is much larger than corresponding values (6.3 keV) for this configuration in ^{235}U and ^{233}Th . Since the present experiment has produced evidence for new levels at 302, 352, and 490 keV, the nature of the $\frac{1}{2}^+[631]$ band becomes more clear with their assignment to the $I = \frac{5}{2}^+$, $\frac{7}{2}^+$, and $\frac{11}{2}^+$ band members, respectively. The level spacing in this band can now be described approximately by the parameters $A=6.78$ keV and $a = +0.12$. All of the levels assigned to this band were observed in the (d,p) spectrum.

Experimental values for the decoupling parameter of this orbital have been reported for 11 actinide nuclei⁴⁰ and are plotted as a function of mass number A in Fig. 9. Be-

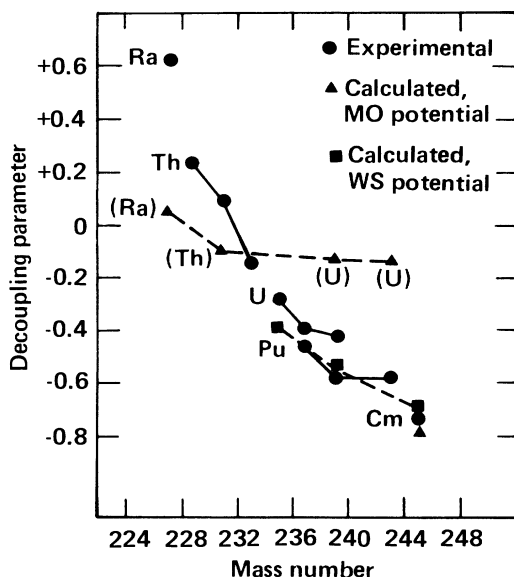


FIG. 9. Experimental and calculated values for the decoupling parameter of the $\frac{1}{2}^+$ [631] band in actinide nuclei.

ginning with the value for ^{227}Ra , +0.62, these parameters show a regular trend, becoming more negative with increasing A . The new experimental value for ^{231}Th is consistent with this trend.

Of the calculated values shown, those from Chasman *et al.*⁴⁰ (Woods-Saxon potential) agree well with experiment, particularly for the two heavier nuclides ^{239}Pu and ^{245}Cm . In the present work, decoupling parameters were calculated employing a modified oscillator potential and assuming ground-state deformations as reported in the literature,⁴¹ for the following nuclei: ^{227}Ra ($\epsilon_2=0.16$, $\epsilon_4=-0.058$), ^{231}Th ($\epsilon_2=0.19$, $\epsilon_4=-0.060$), ^{239}Pu ($\epsilon_2=0.21$, $\epsilon_4=-0.039$), ^{243}Pu ($\epsilon_2=0.22$, $\epsilon_4=-0.024$), and ^{245}Cm ($\epsilon_2=0.23$, $\epsilon_4=-0.021$). As can be seen in the figure, good agreement with experiment is obtained only for ^{245}Cm . The $\frac{1}{2}^+$ [631] decoupling parameter is quite sensitive to hexadecupole deformation (e.g., see the discussion by Chasman *et al.*⁴⁰). Thus, one can obtain agreement with experiment for ^{231}Th by reducing the amount of hexadecupole deformation to $\epsilon_4=-0.01$. Whether this result should be considered evidence that ^{231}Th in the $\frac{1}{2}^+$ [631] state has less hexadecupole deformation than in its ground state, or that the calculated ground state deformation is somehow incorrect, is difficult to decide. In assessing the effect of configuration changes on nuclear shape, Nielsen and Bunker⁴² obtained differences in ϵ_4 of less than 0.02 units when calculating excited-state versus ground-state deformation.

4. $\frac{5}{2}^+$ [622]: 317, 378, 449, and 530 keV

This orbital has not been identified in previous studies of ^{231}Th . Various calculations (given in Table VII) place the bandhead at 420, 470, and 790 keV. The levels at 317 and 378 keV, which are proposed to be the first two

members of the band, have experimentally deduced spin and parity assignments that are consistent with $I^\pi=\frac{5}{2}^+$ and $\frac{7}{2}^+$. All four levels are observed in the (d,p) spectrum; the 449-keV level, in particular, is strongly populated and its angular distribution data are consistent with an angular momentum transfer of $l=4$.

In studying the $^{232}\text{Th}(d,t)^{231}\text{Th}$ reaction, Grottdal *et al.*¹⁵ observed peaks corresponding to the 378- and 449-keV levels and assigned them $\frac{11}{2}^+\frac{3}{2}$ [631] and $\frac{9}{2}^+\frac{1}{2}$ [631] configurations, respectively. Neither assignment is consistent with the energy spacings expected in these rotational bands as constructed in this work. Thus, these peaks are assigned here to the $\frac{5}{2}^+$ [622] band. Even though the predominantly particle nature of the band is demonstrated by the large value for the ratio of (d,p)/(d,t) reaction cross sections, population of the 378- and 449-keV levels by the (d,t) reaction occurs apparently because of the diffuseness of the Fermi surface and the Coriolis interaction.

5. $\frac{7}{2}^+$ [624]: 511 and 580 keV

This orbital has not been assigned in previous studies of ^{231}Th . Calculations (Table VII) place the bandhead variously at 520, 560, and 830 keV. In the $N=133$ nucleus ^{233}Th , the $\frac{7}{2}^+$ [624] bandhead is found at 337 keV,¹⁹ and the levels of this band mix strongly with those of the $\frac{5}{2}^+$ [633] orbital, for which the bandhead energy is 262 keV. Evidence for the existence of the $\frac{7}{2}^+$ [624] band in ^{231}Th was obtained from the observation of an intense peak at 579 keV in the (d,p) spectrum. This level is assigned to the $I=\frac{9}{2}$ member of the band, based on calculated cross sections for its (d,p) population and expected energy. The $\frac{7}{2}^+$ level in this band is expected at approximately 511 keV, an energy where a gamma transition to the ground state will be masked by the relatively intense annihilation radiation peak in the spectrum. A gamma line is found, however, at 468.94 keV, corresponding to the decay of a 510.89 keV level to the 42-keV $\frac{7}{2}^+$ level of the ground state band. Thus, the energy of the $\frac{7}{2}^+$ bandhead level for this orbital is tentatively assigned as 511 keV.

6. Three $K^\pi=\frac{1}{2}^+$ bands: 688, 709, and 735 keV; 793, 809, 854, 890, 970, and 1033 keV; 821 and 839 keV

In the experimental data of Table II, there are 14 γ rays ranging in energy from 436 to 855 keV whose conversion coefficients are markedly higher (by factors of 1.5–15 times) than theoretical values for $M1$ transitions. These large coefficients are ascribed to the presence of an appreciable $E0$ component in each transition. Since pure $E0$ transitions can proceed only via the emission of conversion electrons, their role in enhancing conversion coefficients when $E0+M1$ (+ $E2$) mixing occurs is clear. There are, of course, possible alternative explanations for the existence of large conversion coefficients; the observed transitions could be of higher order multipolarity than either $M1$ or $E2$, or could be strongly hindered $E1$ transitions. These possibilities are unlikely because the ob-

served L -subshell ratios support the $E0$ components and the γ -branching ratios and deduced spins of the levels favor low multiplicities.

Six of these $E0+M1$ (+ $E2$) transitions form part of the evidence for the existence of new levels in ^{231}Th at 688, 709, 793, 809, 821, and 839 keV; each transition feeds either the $I = \frac{1}{2}$ or $\frac{3}{2}$ level of the $\frac{1}{2}^+[631]$ configuration. These new levels, then, are interpreted as being the lowest-lying members of three new $K^\pi = \frac{1}{2}^+$ rotational bands. The $E0$ components in the depopulating transitions indicate that each of the three new rotational bands contains in its wave function some amount of the configuration $(\frac{1}{2}^+[631] \times 0^+)$. If it is assumed that each transition is an $E0+M1$ mixture (i.e., neglecting $E2$ admixtures and recognizing that such an assumption is unphysical, but serves to simplify the discussion), the transitions depopulating the 687-keV band contain 10–20% $E0$ components, those depopulating the 793-keV band 50% $E0$, and those depopulating the 821-keV band 40% $E0$.

Although the $E0$ deexcitation mode is possible between any two levels with the same spin and parity, ordinarily it is much slower than the $M1$ and $E2$ components of the transition. Therefore, observation of transitions with identifiable $E0$ strength is a rather infrequent occurrence in odd- A nuclei. But, when the wave function of the upper level includes an appreciable $K=0$ vibrational component that is coupled to the quasiparticle state predominant in the wave function of the lower level, the $E0$ transition becomes a much more favored mode of decay. Attributing observed $E0$ strength in an odd- A nucleus to β -vibrational character is a natural extension of the observation of β -vibrational 0^+ states in even-even nuclei. Other explanations exist for the nature of 0^+ states, namely their description as particle-hole excitations or pairing vibrations. Both of these forms of excitation are expected to occur somewhere near or above 1 MeV.⁴³ The excitation energies for the first excited 0^+ states in even-mass Th and U nuclei (e.g., at 635 and 730 keV for ^{230}Th and ^{232}Th , respectively) appear to be too low for either of these alternatives. Thus, the $E0$ strength seen in the transitions from low-lying levels in ^{231}Th most probably indicates the presence of some γ -vibrational character.

The characteristics of levels arising from single particle-phonon mixing in odd- A deformed nuclei have been calculated by the Soloviev group.³⁹ In comparing these calculations with experiment, one finds that Ivanova *et al.*³⁹ do not predict the presence of three $\frac{1}{2}^+$ bands in ^{231}Th with phonon-mixed states based upon the $\frac{1}{2}^+[631]$ single particle state. In fact, in the range 250–1020 keV there is predicted just one $K^\pi = \frac{1}{2}^+$ band at 610 keV with the components 50% $\frac{1}{2}^+[640]$ and 30% $(\frac{1}{2}^+[640] \times 0^+)$. It is clear the calculations fail with respect to such details as the degree of fragmentation observed for the $(\frac{1}{2}^+[631] \times 0^+)$ state.

Recognizing that these states are mixing to perhaps an unexpected degree, one can try to identify other components in the wave functions. For example, one can examine the deexciting transitions in an analogous way for evidence of $K=2$ phonon-coupled configurations. All of the new $\frac{1}{2}^+$ and $\frac{3}{2}^+$ levels just discussed (except one) also

decay to the ground state band. One finds for the 688-keV $\frac{1}{2}^+$ level that 82% of its depopulation strength feeds the ground state band with half of this occurring through an $E2$ transition that competes with several other transitions which are of predominantly $M1$ multipolarity. This observation, then, is indicative of a γ -vibrational $(\frac{3}{2}^+[633] \times 2^+)$ component in the wave function of this band. Similarly, one might expect to observe the $(\frac{3}{2}^+[631] \times 2^+)$ configuration mixing into the $K = \frac{1}{2}^+$ bands. Since most of the transitions detected that feed the levels of the $\frac{3}{2}^+[631]$ band at 221 keV are of pure $M1$ multipolarity, there appears to be no evidence for coupling of this single particle state with a γ -vibration.

If the new $K = \frac{1}{2}^+$ bands have some $\frac{1}{2}^+[640]$ character, noticeable features would be strong decay to the $\frac{3}{2}^+[631]$ band (at 221 keV) and population of some of the levels by the (d,t) reaction. In constructing the band at 793 keV, all of the higher spin members, $I > 3/2$, were previously observed in the (d,t) spectrum¹⁵ which is generally consistent with the calculated relative intensities for this band. The previous assignment of levels to this band¹⁵ implied a decoupling parameter $a = -1.89$, which is inconsistent with predicted values,⁴⁰ and, consequently, an $I = \frac{3}{2}$ bandhead at approximately 590 keV which is not found in the present experiment.

Thus, the predominant configuration occurring in each of these $K = \frac{1}{2}^+$ bands can be assigned, as follows: $(\frac{1}{2}^+[631] \times 0^+)$, 821-keV band; $(\frac{3}{2}^+[633] \times 2^+)$, 688-keV band; $\frac{1}{2}^+[640]$, 793-keV band. This analysis suggests the $K^\pi = \frac{1}{2}^+$ states observed experimentally in ^{231}Th are more complex than expected from model calculations.

7. Coriolis mixing of positive-parity bands

For the five positive-parity bands which have been assigned to levels below 500 keV, it is expected that Coriolis mixing causes appreciable perturbation of some level energies. This effect was explicitly included in a calculation done by fitting the observed level energies to standard rotational level-spacing formulae. Also included in the calculation was the $\frac{1}{2}^+[640]$ band at 793 keV. Although calculated values for Coriolis matrix elements are available,⁴⁰ the strength of most of these were determined in the level fitting process.

In the calculation, results of which are listed in Table VIII, a total of 25 level energies were fitted with a standard deviation of 0.5 keV. Values of 13 variable parameters, those listed in Table VIII plus five bandhead energies, were determined. For the decoupling constant of the $\frac{1}{2}^+[640]$ band, a value $a = -0.25$ was obtained, as compared with a calculated value of $a = +0.16$.⁴⁰ The decoupling constant for the $\frac{1}{2}^+[631]$ band derived in this calculation, $a = +0.09$, is little changed from that obtained by a simple fitting of the lowest three band members, neglecting Coriolis mixing. The Coriolis matrix elements derived from this calculation are effective values where the reduction due to inclusion of a pairing factor has not been explicitly removed. These matrix elements show empirical values that are 15–60% of the theoretical.

TABLE VIII. Level-energy fitting calculation for positive-parity bands in ^{231}Th , including Coriolis mixing effects.

	$\frac{5}{2}^+[633]$		$\frac{3}{2}^+[631]$		$\frac{1}{2}^+[631]$		$\frac{5}{2}^+[622]$		$\frac{7}{2}^+[624]$		$\frac{1}{2}^+[640]$	
	E_{expt}	E_{calc}	E_{expt}	E_{calc}	E_{expt}	E_{calc}	E_{expt}	E_{calc}	E_{expt}	E_{calc}	E_{expt}	E_{calc}
	Level energies (keV)											
$E(\frac{1}{2}^-)$					247.6	247.7					793.0	792.3
$E(\frac{3}{2}^-)$			221.4	220.7	272.2	271.5					808.5	808.7
$E(\frac{5}{2}^-)$	0.0	0.0	240.9	241.7	301.7	302.0	317.1	317.8			854	853.0
$E(\frac{7}{2}^-)$	42.0	42.0	275.4	276.9	351.5	352.7	377.6	376.0	510.9	510.9	890.0	891.6
$E(\frac{9}{2}^-)$	96.1	96.1	324.9	323.2		409.5	449	447.9	579	579.1	970	970.9
$E(\frac{11}{2}^-)$	161.9	162.1	385.7	385.8	490	489.3	530	531.5		662.2	1033	1032.0
	Fitted parameters (keV)											
	(theoretical values ^a in parentheses)											
$E(K)$		-0.1		220.5		247.5		317.6		510.7		792.1
Decoupling												
parameter a					+ 0.09	(-0.39)					-0.25	(+ 0.16)
	$\langle \frac{1}{2}[640] j_- \frac{1}{2}[631] \rangle = -0.38$								$\langle \frac{3}{2}[631] j_- \frac{5}{2}[622] \rangle = 1.6$ (4.8)			
	$\langle \frac{1}{2}[640] j_- \frac{3}{2}[631] \rangle = 2.2$ (4.6)								$\langle \frac{5}{2}[633] j_- \frac{7}{2}[624] \rangle = 2.7$ (4.6)			
	$\langle \frac{1}{2}[631] j_- \frac{3}{2}[631] \rangle = 0.79$ (0.39)								$A = 6.79$			
	Fixed parameters (keV)											
	(theoretical values ^a in parentheses)											
	$\langle \frac{3}{2}[631] j_- \frac{5}{2}[633] \rangle = 0.23$ (0.46)								$\langle \frac{5}{2}[622] j_- \frac{7}{2}[624] \rangle = 0.05$ (0.005)			

^aFrom Ref. 40.

This empirical reduction of matrix elements is, by now, a common feature of such calculations.⁴⁰ An exception to this behavior is the $\frac{1}{2}^+[631]-\frac{3}{2}^+[631]$ matrix element where the empirical value, 0.8 keV, is twice the calculated value.

8. ($\frac{3}{2}^+[631] \times 0^+$): 961 keV

The 961 keV $\frac{3}{2}^+$ level is well established by many depopulating transitions. The transition to the $\frac{3}{2}^+ \frac{3}{2}^+[631]$ level has an $E0$ component. Therefore, based on our previous discussion (in Sec. IV B 6) of the nuclear structure thought to give rise to such mixed $E0 (+ M1 + E2)$ transitions, we assign this level tentatively to the $K^\pi = 0^+$ vibration on the $\frac{3}{2}^+[631]$ band.

C. Negative parity bands

1. $\frac{5}{2}^- [752]$: 186, 205, 237, 278, 335, and 403 keV

In previous studies of ^{235}U α decay⁴⁻⁸ and the (d,t) and ($^3\text{He}, \alpha$) reactions,¹³⁻¹⁵ the levels listed above have been established as the first six members of the $\frac{5}{2}^- [752]$ rotational band. Transitions that feed or depopulate the three lowest of these have been identified in the present (n, γ) study. All but the 237-keV level are populated in the present (d,p) measurement.

2. $\frac{7}{2}^- [743]$: 388, 452, 530, and 704 keV

In previous studies of ^{235}U alpha decay,⁴⁻⁸ the 388- and 452-keV levels were established as the first two members of the $\frac{7}{2}^- [743]$ rotational band. Transitions feeding and depopulating the 388-keV level have been identified in the present (n, γ) study. The levels at 530 and 704 keV, which are populated in the present (d,p) measurement, are assigned to the $I = \frac{11}{2}$ and $\frac{15}{2}$ members of the band. It will be shown that the energies of all these levels are well fitted by a calculation that includes the effect of Coriolis mixing among the bands arising from the $j_{15/2}$ spherical orbital.

3. $\frac{1}{2}^- [501]$: 555, 594, and 596 keV

Experimental evidence for this orbital has been found in many actinide nuclei ranging from ^{227}Ra to ^{249}Cm ,⁴⁴ where the expected signature is strong population of the $I = \frac{1}{2}$ and $\frac{3}{2}$ levels by the (d,t) reaction. In ^{231}Th this band was identified in (d,t) studies, first by Boyno *et al.*,¹⁴ who assigned observed levels at 558 and 594 keV to the $I = \frac{1}{2}$ and ($\frac{3}{2}, \frac{5}{2}$) members of the band. The calculated energy for this orbital is sensitive to the choice of single-particle potential. Two of the entries in Table VII (folded Yukawa and Woods-Saxon potential calculations) bracket the experimental energy for this orbital rather well. The calculated decoupling constant of Chasman *et al.*⁴⁰ implies a level spacing of 4 keV for the $\frac{3}{2}-\frac{5}{2}$ levels.

In the present work, the $\frac{1}{2}^- [501]$ orbital is assigned to

the three levels indicated above; from these, one calculates a rotational parameter $A=6.73$ keV and a decoupling parameter $a=+0.93$. The experimental observation that ^{231}Ac β decay populates levels at $554(\frac{1}{2}^-)$ and $593(\frac{3}{2}^-)$ keV is consistent with the $\frac{1}{2}^+[400]$ ground state assignment to ^{231}Ac .

4. $\frac{3}{2}^- [761]$: 591, 629, 656, and 1084 keV

For this orbital, calculated bandhead energies are in the range 650–750 keV (Table VII). The experimentally observed $I^\pi=\frac{3}{2}^-$ level at 590.836 keV is assigned as the bandhead. The predominant mode of deexcitation (96%) of this level is to the first two levels of the $\frac{5}{2}^- [752]$ band. A level at 629.339 keV, which also decays mainly (87%) to the same two levels, is assigned as the $\frac{5}{2}$ member of the band. The $I=\frac{7}{2}$ member of this band is assigned to a level at 655.92 keV on the basis of two transitions that feed levels of the $\frac{5}{2}^- [752]$ band. These experimentally observed level energies are reproduced rather well in the calculation that includes the effect of Coriolis mixing among the bands of the $j_{15/2}$ spherical orbital (see below).

It is interesting that two $I^\pi=\frac{3}{2}^-$ levels at 591 and 594 keV occur so close to one another. From their proximity one can derive an experimental upper limit of 0.1 keV for the Coriolis matrix element describing the interaction. This result is consistent with the orbital assignments $\frac{3}{2}^- [761]$ and $\frac{1}{2}^- [501]$: Chasman *et al.*⁴⁰ calculate a $\langle j_+ \rangle$ matrix element of -0.11 keV for this orbital pair.

5. $\frac{1}{2}^- [770]$: 714($\frac{3}{2}$), 720($\frac{7}{2}$), 813($\frac{15}{2}$),
and 833($\frac{1}{2}$) keV

The expected characteristics of this orbital are the following: (a) Bandhead energies calculated variously at 760, 1150, and 1290 keV (Table VII); Ivanova *et al.*³⁹ predict this orbital to occur at 760 keV, just 40 keV above the $\frac{3}{2}^- [761]$ band. (b) A calculated decoupling parameter of $a=-7.3$ keV; this implies that the $\frac{3}{2}^-$ level lies below the $\frac{1}{2}$ level for this band and a $\frac{1}{2}-\frac{3}{2}$ level spacing of 120 keV, neglecting any variation caused by Coriolis effects. (c) Both the $I=\frac{1}{2}$ and $\frac{3}{2}$ levels will be populated in the ARC measurements. (d) Calculated cross sections for higher-spin members of the band are low enough that they will be difficult to identify in the (d,t) spectrum. With these characteristics as a guide, levels populated in the ARC measurement were examined with respect to which levels show appreciable deexcitation to the $\frac{3}{2}^- [761]$ and $\frac{5}{2}^- [752]$ bands. The most likely candidates were the following: (a) As the $\frac{3}{2}$ level, those at 620, 714, and 1074 keV, and (b) as the $\frac{1}{2}$ level, those at 833 and 1160 keV. Since it is known that this band will interact strongly with the $\frac{3}{2}^- [761]$ band, assignment of experimental levels as members of the bands was accomplished in the course of an explicit calculation of Coriolis mixing described next.

6. Coriolis mixing of negative-parity bands

Selected pairs of the candidate levels were assigned to the $I=\frac{1}{2}$ and $\frac{3}{2}$ members of the $\frac{1}{2}^- [770]$ band and were

used in calculations to fit 18 level energies among four $j_{15/2}$ orbitals (Table IX); Coriolis interactions were explicitly included. The result was that the best candidates for the low-spin members of the $\frac{1}{2}^- [770]$ band are the 714 keV–833 keV pair. The findings that support this assignment are (a) a large fraction of the deexcitation of the 714-keV level populates members of the $\frac{5}{2}^- [752]$ band, (b) a satisfactory fit to experimental levels, and (c) parameters derived from the best fit to these levels ($a=-7.2$, Coriolis matrix elements for the $\frac{3}{2}-\frac{5}{2}$ and $\frac{5}{2}-\frac{7}{2}$ band interactions approximately 50% of the theoretical) correspond to what is expected from the theoretical calculation and experience. On the other hand, certain aspects of this interpretation are not in accord with expectation, as follows: (a) Transitions between the 714-keV level and members of the $\frac{3}{2}^- [761]$ band have not been detected; (b) the fitted Coriolis matrix element for the $\frac{1}{2}-\frac{3}{2}$ band pair is only 18% of theoretical, while the fitted decoupling parameter for the $\frac{1}{2}^- [770]$ band is 100% of the theoretical. Thus, the assignment of the indicated levels as members of the $\frac{1}{2}^- [770]$ band is made based on a plausible interpretation of the experimental observations.

7. ($\frac{3}{2}^+ [631] \times 0^-$): 620 keV

Studies of the neighboring nuclei ^{233}Th , ^{235}U , and ^{239}U have shown evidence for an octupole vibration coupled to the $\frac{1}{2}^+ [631]$ band, resulting in levels with excitations in the range 600–800 keV.^{17,44} In ^{233}Th , there has also been found evidence for the coupling of an octupole vibration to the $\frac{3}{2}^+ [631]$ particle state. Although no $\frac{1}{2}^-$ levels found in the present work have been assigned as octupole vibrations, a $\frac{3}{2}^-$ state is found at 620 keV that could be such a configuration since it is not assigned to other negative parity bands and decays in part to the $\frac{3}{2}^+ [631]$ band. This state is assigned tentatively as the first member of a band consisting of an octupole vibration coupled to the $\frac{3}{2}^+ [631]$ band.

8. ($\frac{5}{2}^- [752] \times 0^+$): 624 and 634 keV

Each of these levels is depopulated by two transitions that lead to the lowest two levels of the $\frac{5}{2}^- [752]$ band at 186 keV. One of each pair of transitions has experimentally demonstrated $M1+E0$ character. These levels can be interpreted as members of a new rotational band with ($\frac{5}{2}^- [752] \times 0^+$) character. The level spacing here is 10 keV, which is about half of that found in the base state band. The large apparent moment of inertia for the base state band is understood in terms of a general compression of the band due to Coriolis mixing with levels of the nearby $\frac{7}{2}^- [743]$ band. Presumably, the 0^+ vibrational bands built on these two base states could also be strongly mixed, which would account for the observed level spacing. Since the evidence for this quasiparticle-phonon coupled band is not very extensive, its existence and configurational assignment must be considered tentative.

TABLE IX. Level-energy fitting calculation for negative-parity bands in ^{231}Th , including Coriolis mixing effects.

	$\frac{5}{2}^- [752]$		$\frac{7}{2}^- [743]$		$\frac{3}{2}^- [761]$		$\frac{1}{2}^- [770]$		$\frac{9}{2}^- [734]$	
	E_{expt}	E_{calc}	E_{expt}	E_{calc}	E_{expt}	E_{calc}	E_{expt}	E_{calc}	E_{expt}	E_{calc}
Level energies (keV)										
$E(\frac{1}{2}^-)$							833.2	833.5		
$E(\frac{3}{2}^-)$					590.8	588.6	713.8	711.6		
$E(\frac{5}{2}^-)$	185.7	185.1			629.3	629.3		984.2		
$E(\frac{7}{2}^-)$	205.3	205.5	387.8	388.6	656.0	658.5	720.3	723.0		
$E(\frac{9}{2}^-)$	236.9	237.2	452.2	452.9		756.3		1188.9		918.6
$E(\frac{11}{2}^-)$	277.8	280.4	530	527.2		865.1		715.4		1005.5
$E(\frac{13}{2}^-)$	335	331.6		598.9		945.2		1447.3		1106.4
$E(\frac{15}{2}^-)$	403	403.9	704	705.4	1084	1083.5	813	812.2		1225.9
Fitted parameters (keV)										
(theoretical values ^a in parentheses)										
$E(K)$		185.5		372.4		591.7		833.2		918.2
Decoupling										
parameter a										
							-7.2	(-7.3)		
	$\langle \frac{1}{2}^- [770] j_- \frac{3}{2}^- [761] \rangle = 1.3$	(7.3)					$\langle \frac{5}{2}^- [752] j_- \frac{7}{2}^- [743] \rangle = 3.0$	(7.2)		
	$\langle \frac{3}{2}^- [761] j_- \frac{5}{2}^- [752] \rangle = 3.7$	(7.3)						$A = 6.67$		
Fixed parameters (keV)										
(theoretical values ^a in parentheses)										
	$\langle \frac{7}{2}^- [743] j_- \frac{9}{2}^- [734] \rangle = 3.4$	(6.8)								

^aFrom Ref. 40.9. $\frac{5}{2}^- [503]$: 685 keV

Evidence for a level at 684.5 keV is provided by two γ transitions leading to the first two levels of the $\frac{5}{2}^+ [752]$ band and by population in the (d,p) and (d,t) reactions. Model-independent considerations suggest $I = \frac{3}{2}^-$ to $\frac{7}{2}^-$ with negative parity for the level. In the calculations of Möller *et al.*³⁸ (folded Yukawa potential), a $\frac{5}{2}^- [503]$ band is found at 960 keV, which mixes appreciably through $\Delta N=2$ mixing with the $\frac{5}{2}^- [752]$ band; the predominance of the observed transition to the 185-keV $\frac{5}{2}^-$ level in our work is consistent with this description. In the calculations of Ivanova *et al.*,³⁹ a $\frac{5}{2}^-$ band is found at 950 keV, the only such band other than the $\frac{5}{2}^- [752]$ configuration. It is of collective rather than single-particle nature, consisting predominantly of a β vibration coupled to the $\frac{5}{2}^- [752]$ band. In the present work, the experimental conversion coefficient for the intense 499-keV transition depopulating the level indicates no evidence for $E0$ mixing in the transition; thus, a strong contribution from the vibrational configuration $\frac{5}{2}^- [752] \times 0^+$ is unlikely.

10. $\frac{3}{2}^+ [501]$: 876 and 915 keV

Grotdal *et al.*¹⁵ observed levels at 869, 908, and 965 keV and assigned these strong (d,t) lines to the lowest

members of the $\frac{3}{2}^- [501]$ rotational band. In agreement with this, levels at 876 and 915 keV observed in the (n, γ) part of the present work are assigned tentatively as the $\frac{3}{2}^-$ and $\frac{5}{2}^-$ members of the band, assuming an energy discrepancy of 7 keV with the energy calibrations of the previous (d,t) measurement.

D. (d,p) population of rotational bands

Angular distributions for several of the more intense lines in the (d,p) spectrum are shown in Fig. 4. The experimental data show reasonable agreement with the expected angular distribution, based on the assigned spin and parity of the populated level. Generally, however, it was not possible to make unambiguous assignments of angular momentum transfer for new levels in the (d,p) spectrum in the absence of other kinds of experimental evidence regarding spin and parity. Examples of such levels shown in Fig. 4 are those at 403, 449, and 579 keV. Each of these has been observed only in transfer reactions and their spin and parity assignments must be considered as tentative, although the prominence of the 403-keV level in the ($^3\text{He},\alpha$) reaction spectrum is indicative of large l transfer and, thus, serves to verify its configuration assignment. On this basis, we rate the confidence of this as-

segment as probable, rather than tentative.

Configuration assignments for certain levels populated by the (d,p) reaction are listed in Table X. Cross sections were calculated using the DWUCK code with optical model parameters taken from an earlier calculation for $^{232}\text{Th}(d,p)$ by Grotdal *et al.*¹⁵ In the present calculation, wave functions were generated with a modified oscillator potential described by the parameters $\kappa=0.05$ and $\mu=0.448$. In previous (d,p) and (d,t) studies of ^{231}Th ,¹⁴⁻¹⁶ it has been shown that cross sections calculated with the use of these parameters show better correspondence with experiment than those obtained using parameters recommended in more recent papers on the oscillator potential, $\kappa=0.0635$ and $\mu=0.339$ (Ref. 41). The controlling factor here is the lower value of κ , which determines the amount of spin-orbit coupling in the Hamiltonian. In the present calculations, the spherical orbits $g_{9/2}$ and $i_{11/2}$ are closer to each other in energy than for $\kappa=0.0635$. Thus, when in a deformed potential, the Nilsson states originating in these spherical orbits, $\frac{3}{2}^+[633]$, $\frac{7}{2}^+[624]$ and $\frac{3}{2}^+[631]$, $\frac{5}{2}^+[622]$, mix to a greater extent than otherwise. Since these orbitals "cross" in a Nilsson diagram, the effect of this "crossing" is for the $\frac{3}{2}^+[631]$ and $\frac{5}{2}^+[622]$ bands to take on the character of $g_{9/2}$ bands to some degree and, thus, to show greater (d,p) strength to the $I=\frac{9}{2}$ states than otherwise. In a corresponding manner, the (d,p) strength feeding $I=\frac{11}{2}$ states in the $\frac{5}{2}^+[633]$ and $\frac{7}{2}^+[624]$ bands will be enhanced. In contrast to this behavior, the wave functions calculated for the $\frac{1}{2}^+[631]$ orbital are little affected by parameter choice.

In comparing the experimental and calculated cross sections listed in Table X, it can be seen that in several instances the inclusion of Coriolis mixing is essential to good agreement. A vivid illustration of this is found for the $I=\frac{9}{2}$ levels of the positive-parity orbitals where, for the $\frac{3}{2}^+[631]$, $\frac{1}{2}^+[631]$, and $\frac{5}{2}^+[622]$ bands, use of Coriolis-mixed wave functions produces dramatic improvement. In other instances, the effect of Coriolis mixing seems to be acting in the wrong direction, as, e.g., in the case of the positive parity $I=\frac{5}{2}$ levels of the $\frac{3}{2}^+[631]$ and $\frac{1}{2}^+[631]$ bands where the mixed wave functions produce increased strength in the $\frac{1}{2}^+[631]$ band, while experimentally it is found in the $\frac{3}{2}^+[631]$ band. Overall, there is reasonable agreement between the experimental and calculated cross sections (with Coriolis mixing) for the positive-parity bands. The total experimental (d,p) strength for these bands agrees with that calculated to about 10%, another indication that appropriate configuration assignments have been made. For the negative-parity bands, the total experimental (d,p) strength exceeds that calculated by a factor of 3, even after some enhancement in the latter due to Coriolis mixing. The calculated cross sections underestimate experiment by a factor of 2 for the two $I=\frac{15}{2}$ levels, where the great majority of the spectroscopic strength lies. In this case, the source of the discrepancy must be other than in the correction for pairing effects since these bands ($\frac{5}{2}^-[752]$ and $\frac{7}{2}^-[743]$) lie on opposite sides of the Fermi surface and have quite different occupation factors ($u^2=0.20$ and 0.88 , respective-

ly).

An important result of our (d,p) measurement is that it provides valuable corroboratory evidence for the positive-parity level sequence observed at rather low excitation in ^{231}Th . The observation in the (n, γ) experiment on nine levels, ranging from 221 to 378 keV and belonging to the orbitals $\frac{3}{2}^+[631]$, $\frac{1}{2}^+[631]$, and $\frac{5}{2}^+[622]$, is proposed. Evidence for each of these was detected in the (d,p) spectrum.

V. CONCLUSIONS

This comprehensive study of ^{231}Th has resulted in the assignment of 18 single-particle or mixed vibrational configurations. The corresponding rotational bands contain 57 levels. These levels have been established and identified by secondary (n, γ) transitions, by primary transitions from thermal and average resonance neutron capture (ARC), and by (d,p) and (d,t) reactions. Additional levels without assignments are suggested. A total of 157 transitions (out of 278 measured secondary lines) are placed in the level scheme. All expected Nilsson states were observed below 750 keV. The level scheme is essentially complete concerning $\frac{1}{2}$ and $\frac{3}{2}$ states below 700 keV due to the ARC data.

A special feature of the level scheme is the appearance of some admixture of the $K^\pi=0^+$ β vibration built on a $\frac{1}{2}^+[631]$ Nilsson state in three rotational bands which lie within 140 keV of each other. This fragmentation was unexpected theoretically and is the explanation for the observation of an unusually large number of $E0$ transitions.

As indications of stable octupole deformation in odd- A nuclei in this mass region, two criteria have been suggested: (a) Rotational bands with degenerate parity doublets;¹ in some cases, enhancement of $E1$ transitions between the bands of a parity doublet were observed;³ (b) for $K=\frac{1}{2}$ bands, a hybridization of the decoupling parameters, i.e., the decoupling parameters have the same absolute value, but with opposite sign, was predicted⁴⁵ and observed experimentally.² In the present work no particularly close parity doublets are present. This result is in accordance with calculations¹ that predict the occurrence of such doublets to be less likely in ^{231}Th than in the more favorable cases of ^{229}Th and ^{227}Th . In ^{231}Th only the $\frac{5}{2}^-[752]$ and $\frac{1}{2}^-[501]$ bands decay preferentially by $E1$ transitions and, for these, there are no alternate decay modes. With respect to hybridization of decoupling parameters, the decoupling of the $\frac{1}{2}^+[631]$ band is in the direction of hybridization, i.e., the parameter is positive as compared with a predicted negative value. Nevertheless, the decoupling parameters of the observed negative parity bands, $\frac{1}{2}^-[501]$ and $\frac{1}{2}^-[770]$, are close to predicted values based upon pure quadrupole (and hexadecapole) deformation. Thus, on the basis of the stated criteria, no evidence is found for significant stable octupole deformation in ^{231}Th .

ACKNOWLEDGMENTS

One of the authors (D.H.W.) wishes to express thanks to the Institut Laue-Langevin, the Heineman Foundation,

TABLE X. Experimental and calculated differential cross sections for the $^{230}\text{Th}(d,p)^{231}\text{Th}$ reaction; $E_d=20$ MeV, $\theta=40^\circ$.

Spin	E_{expt}	$\frac{5}{2}^+ [633]$			$\frac{3}{2}^+ [631]$			$\frac{1}{2}^+ [631]$			$\frac{5}{2}^+ [622]$					
		Expt.	Calc.	Mix	E_{expt}	Expt.	Calc.	Mix	E_{expt}	Expt.	Calc.	Mix	E_{expt}	Expt.	Calc.	Mix
$\frac{1}{2}$																
$\frac{3}{2}$																
$\frac{5}{2}$																
$\frac{7}{2}$																
$\frac{9}{2}$																
$\frac{11}{2}$																
$\frac{13}{2}$																
$\frac{15}{2}$																
$\frac{5}{2}$																
$\frac{7}{2}$																
$\frac{9}{2}$																
$\frac{11}{2}$																
$\frac{13}{2}$																
$\frac{15}{2}$																
$\frac{7}{2}^+ [624]$																
$\frac{5}{2}^- [752]$																
$\frac{7}{2}^- [743]$																
$\frac{5}{2}$																
$\frac{7}{2}$																
$\frac{9}{2}$																
$\frac{11}{2}$																
$\frac{13}{2}$																
$\frac{15}{2}$																

^aThe total intensity of these two peaks was used to normalize experimental and calculated intensities for all of the data. $U^2=0.83$ for this band.

^bBased upon evidence obtained from (n,γ) and other experimental studies, the observed peak in the (d,p) spectrum is a multiplet.

and Western Oregon State College for financial support during his stay in Grenoble. One of the authors (H.G.B.) wishes to express his gratitude to the Lawrence Livermore National Laboratory for financial support during his stay in Livermore. This work was performed, in part, under the auspices of the U.S. Department of Energy by the Lawrence Livermore National Laboratory under Contract No. W-7405-Eng-48, by the Brookhaven National Labora-

tory under Contract No. DE-AC02-78HO0016, by Princeton University under Contract No. EY-76-S-02-2184, and under the auspices of the National Science Foundation by Princeton University under Grant No. PH78-01473. The authors are indebted for the use of ^{230}Th to the Division of Chemical Sciences, Office of Basic Energy Sciences, U.S. Department of Energy, through the Calutron facilities of the Oak Ridge National Laboratory.

- *Permanent address: Western Oregon State College, Monmouth, OR 97361.
- †Permanent address: National Research Council of Canada, Ottawa, Ontario, Canada K1A 0R6.
- ‡Permanent address: Physik-Department, Technische Universität München, 8046 Garching, Federal Republic of Germany.
- §Permanent address: Daresbury Laboratory, Warrington, United Kingdom WA4 4AD.
- **Permanent address: Centre d'Etudes Nucleaires Grenoble/LETI, 38041 Grenoble, France.
- ††Permanent address: Centre d'Etudes Nucleaires, Bordeaux-Gradignan, France.
- ‡‡Permanent address: Los Alamos National Laboratory, Los Alamos, NM 87545.
- §§Permanent address: Savannah River Laboratory, E. I. Dupont De Nemours and Co., Aiken, SC 29808.
- ¹R. R. Chasman, *Phys. Lett.* **96B**, 7 (1980).
- ²R. K. Sheline, D. Decman, K. Nybø, T. F. Thorsteinsen, G. Løvholden, E. R. Flynn, J. A. Cizewski, D. K. Burke, G. Sletten, P. Hill, N. Kaffrell, W. Kurcewicz, G. Nyman, and G. Leander, *Phys. Lett.* **133B**, 13 (1983).
- ³I. Ahmad, R. R. Chasman, J. E. Gindler, and A. M. Friedman, *Phys. Rev. Lett.* **52**, 503 (1984).
- ⁴L. A. Kroger, C. W. Reich, and J. E. Klein, Aerojet Nuclear Co. (Idaho Falls, ID), Report No. ANCR-1016, p. 75, 1971.
- ⁵R. L. Heath, Aerojet Nuclear Co. (Idaho Falls, ID), Report No. ANCR-1000-2, 1974.
- ⁶W. Tech, R. D. Conner, and R. H. Betts, *Nucl. Phys.* **A228**, 432 (1974).
- ⁷E. Vano, R. Gaeta, L. Gonzales, and C. F. Liang, *Nucl. Phys.* **A251**, 225 (1975).
- ⁸S. A. Baranov, V. M. Shatinskii, A. G. Zelenkov, and V. A. Pchelin, *Yad. Fiz.* **26**, 921 (1977) [*Sov. J. Nucl. Phys.* **26**, 486 (1977)].
- ⁹K. Takahashi and H. Morinaga, *Nucl. Phys.* **21**, 133 (1960).
- ¹⁰T. Yamamoto, T. Wakabayasi, Y. Takeda, S. Itagaki, and O. Konno, *Res. Rep. Lab. Nucl. Sci., Tohoku Univ.* **4**, No. 1, 53 (1971).
- ¹¹K. Chayawattanangkur, G. Herrmann, and N. Trautmann, *J. Inorg. Nucl. Chem.* **35**, 3061 (1973).
- ¹²T. H. Braid, R. R. Chasman, J. R. Erskine, and A. M. Friedman, *Phys. Lett.* **18**, 149 (1965).
- ¹³T. W. Elze, T. von Egidy, and J. R. Huizenga, *Nucl. Phys.* **A128**, 564 (1969).
- ¹⁴J. S. Boyno, T. W. Elze, and J. R. Huizenga, *Nucl. Phys.* **A157**, 263 (1970).
- ¹⁵T. Grottdal, J. Limstrand, K. Nybø, K. Skar, and T. F. Thorsteinsen, *Nucl. Phys.* **A189**, 592 (1972).
- ¹⁶W. Wilcke, W. Feix, Th. W. Elze, J. R. Huizenga, and R. C. Thompson, *Nucl. Phys.* **A286**, 279 (1977).
- ¹⁷T. von Egidy, J. Almeida, G. Barreau, H. G. Börner, W. F. Davidson, R. W. Hoff, P. Jeuch, K. Schreckenbach, D. D. Warner, and D. H. White, *Phys. Lett.* **81B**, 281 (1979).
- ¹⁸T. von Egidy, G. Barreau, H. G. Börner, W. F. Davidson, J. Larysz, D. D. Warner, P. H. M. van Assche, K. Nybø, T. F. Thorsteinsen, G. Løvholden, E. R. Flynn, J. A. Cizewski, R. K. Sheline, D. Decman, D. G. Burke, G. Sletten, N. Kaffrell, W. Kurcewicz, T. Bjørnstad, and G. Nyman, *Nucl. Phys.* **A365**, 26 (1981).
- ¹⁹P. Jeuch, T. von Egidy, K. Schreckenbach, W. Mampe, H. G. Börner, W. F. Davidson, J. A. Pinston, and R. Roussille, *Nucl. Phys.* **A317**, 363 (1979).
- ²⁰J. Almeida, T. von Egidy, P. H. M. van Assche, H. G. Börner, W. F. Davidson, K. Schreckenbach, and A. I. Namenson, *Nucl. Phys.* **A315**, 71 (1979).
- ²¹H. G. Börner, H. R. Koch, H. Seyfarth, T. von Egidy, W. Mampe, J. A. Pinston, K. Schreckenbach, and D. Heck, *Z. Phys. A* **286**, 31 (1978).
- ²²R. W. Hoff, W. F. Davidson, D. D. Warner, H. G. Börner, and T. von Egidy, *Phys. Rev. C* **25**, 2232 (1982).
- ²³H. R. Koch, H. G. Börner, J. A. Pinston, W. F. Davidson, J. Faudou, R. Roussille, and O. W. B. Schult, *Nucl. Instrum. Methods* **175**, 401 (1980).
- ²⁴G. L. Borchert, *Z. Naturforsch.* **31a**, 102 (1976).
- ²⁵E. G. Kessler, R. D. Deslattes, A. Henins, and W. C. Sauder, *Phys. Rev. Lett.* **40**, 171 (1978).
- ²⁶M. R. Schmorak, *Nucl. Data Sheets* **40**, 1 (1983); **21**, 91 (1977).
- ²⁷H. G. Börner, G. Barreau, W. F. Davidson, P. Jeuch, T. von Egidy, J. Almeida, and D. H. White, *Nucl. Instrum. Methods* **166**, 251 (1979).
- ²⁸H. G. Börner, W. F. Davidson, J. Almeida, J. Blachot, J. A. Pinston, and P. H. M. Van Assche, *Nucl. Instrum. Methods* **164**, 579 (1979).
- ²⁹W. Mampe, K. Schreckenbach, J. Jeuch, B. P. K. Maier, F. Braumandl, J. Larysz, and T. von Egidy, *Nucl. Instrum. Methods* **154**, 127 (1978).
- ³⁰R. S. Hager and F. C. Selzer, *Nucl. Data A* **4**, 1 (1978).
- ³¹D. D. Warner, W. F. Davidson, and W. Gelletly, *J. Phys. G* **5**, 1723 (1979).
- ³²M. L. Stelts and R. E. Chrien, *Nucl. Instrum. Methods* **155**, 253 (1978), and private communication.
- ³³R. C. Greenwood and R. E. Chrien, *Nucl. Instrum. Methods* **138**, 125 (1976).
- ³⁴R. E. Chrien, in *Capture Gamma-Ray Spectroscopy and Related Topics—1984*, AIP Conf. Ser. No. 62, edited by S. Raman (AIP, New York, 1985), p. 342.
- ³⁵R. T. Kouzes and W. H. Moore, *Phys. Rev. C* **12**, 1511 (1975).
- ³⁶D. H. White, R. E. Birkett, and T. Thomson, *Nucl. Instrum. Methods* **77**, 261 (1969).
- ³⁷A. H. Wapstra and K. Bos, *At. Data Nucl. Data Tables* **19**, 215 (1977).
- ³⁸P. Möller, S. G. Nilsson, and J. R. Nix, *Nucl. Phys.* **A229**, 292 (1974).
- ³⁹S. P. Ivanova, A. L. Komov, L. A. Malov, and V. G. Soloviev,

- Izv. Akad. Nauk SSSR, Ser. Fiz. **39**, 1612 (1975).
- ⁴⁰R. R. Chasman, I. Ahmad, A. M. Friedman, and J. R. Erskine, *Rev. Mod. Phys.* **49**, 833 (1977).
- ⁴¹I. Lamm, *Nucl. Phys.* **A125**, 504 (1969).
- ⁴²B. S. Nielsen and M. E. Bunker, *Nucl. Phys.* **A245**, 376 (1975).
- ⁴³I. Ragnarsson and R. A. Broglia, *Nucl. Phys.* **A263**, 315 (1976).
- ⁴⁴R. W. Hoff, R. W. Lougheed, G. Barreau, H. Börner, W. F. Davidson, K. Schreckenbach, and D. D. Warner, in *Capture Gamma-Ray Spectroscopy and Related Topics—1984*, Ref. 34, p. 250.
- ⁴⁵A. Bohr and B. R. Mottleson, *Nuclear Structure* (Benjamin, New York, 1975), Vol. 2.